Available online at www.sciencedirect.com
SCIENCE DIRECT®
Coordination Chemistry Reviews 249 (2005) 1536–1554
COORDINATION CHEMISTRY REVIEWS
www.elsevier.com/locate/ccr

Review

Spectroelectrochemistry of hydrogenase enzymes and related compounds

Stephen P. Best *

School of Chemistry, University of Melbourne, Parkville, Melbourne 3010, Vic., Australia

Received 8 December 2004; accepted 23 January 2005
Available online 9 April 2005

Contents

Abstract

The experimental approaches used to conduct IR spectroelectrochemical (SEC) studies from enzymes and inorganic compounds at ambient and elevated gas pressures are described. The application of these techniques to the study of the catalytically active site of [NiFe]- and [FeFe]-hydrogenase enzymes in their different accessible states and to the study of relevant metal complexes is reviewed. Dithiolate bridged diiron compounds provide functional models of the hydrogenases. The application of chemical, electrochemical and SEC techniques to the elucidation of the details of the electrocatalytic proton reduction is described.

Keywords: Hydrogenase; Electrocatalysis; Spectroelectrochemistry; Infrared spectroscopy; Dithiolate bridged diiron carbonyl compounds

1. Introduction

There is no clearer biologically relevant demonstration of the utility to be gained from the conjunction of electrochemical and spectroscopic techniques than from the study of the hydrogenase enzymes. Justification for this assertion derives not from the range of accessible oxidation states, for this is a feature common to a wide range of metalloenzymes, but from the presence of carbon monoxide and cyanide ligands bound to the catalytic centre. These ligands are well known to be as effective infrared (IR) transmitters of the electron richness of

* Tel.: +61 3 83446505; fax: +61 3 93475180.
E-mail address: spbest@unimelb.edu.au.

0010-8545/$ – see front matter © 2005 Elsevier B.V. All rights reserved.
doi:10.1016/j.ccr.2005.01.012

the metals to which they are bound, this being due to: (i) the high sensitivity of the CO and CN force constants to changes in back donation from metal orbitals of local π symmetry into the antibonding π orbital of the diatomic ligand; (ii) the high intensity of the stretching modes of the ligands in the IR spectrum; (iii) the absence of strong absorptions from other molecular species in the portion of the IR spectrum inhabited by the CO and CN stretches. EPR spectroscopy has provided critical insights into the identity of the metal and redox levels of metalloenzymes, particularly the [NiFe]-hydrogenases, however, the presence of EPR silent states limits the extent of information able to be obtained by this approach. Since IR spectra may be obtained from all long-lived redox states of the system these results both enrich and complete the picture able to be extracted for the EPR-active states.

The primary focus of this contribution is the application of spectroelectrochemical (SEC) techniques to hydrogenase enzymes and to the delineation of the chemistry initiated by reduction of compounds related in composition and/or structure to the active sites of the enzyme. For the reasons already outlined the application of IR spectroscopy is of particular importance, and attention will be devoted both to the different experimental approaches that have been applied together with the analysis of the results. The elucidation of the chemistry from mere spectroscopic results leads one on a path that can be poorly illuminated by a single spectroscopic approach. Therefore, it is critically important that the conclusions drawn from the analysis of the SEC results be subject to validation by complementary physical and/or spectroscopic methods. The complexity lurking below the surface of even the supposedly simple model compounds is an exceedingly rich mine both of chemical insights and frustration.

2. General features of the hydrogenase enzymes

Details of the biology and biochemistry of hydrogenase enzymes have been previously reviewed [1–9] and it is not the purpose of this contribution to add to that literature. This section sets out to provide sufficient background for those less familiar with the field to put into context for the following sections.

Efficient catalysis of the reversible oxidation of dihydrogen to give protons is performed primarily by two classes of hydrogenase that are identified according to the metal composition of the catalytically active centre. Both classes feature an electron-transport chain consisting of several iron–sulfur clusters leading to a deeply buried active site [10–15]. The [NiFe]-hydrogenases feature an active site in which the metal atoms are bridged by two cysteinyl sulfur atoms and the Fe atom is additionally co-ordinated by two cyanide groups and one molecule of carbon monoxide (Fig. 1a). In the aerobically isolated inactive form of the enzyme there is an additional bridging ligand that has mostly been modelled as oxide or hydroxide and this is lost from the di-metal centre during activation [16]. For the [FeFe]-hydrogenase the active centre, or H-cluster, consists of a diiron subsite linked through a cysteinyl sulfur atom to a 4Fe4S cluster [17,18]. The diiron subsite, $\{2Fe3S\}_H$, consists of a propane-1,3-dithiolate (pdt) or di(thiomethyl)amine (dta) cofactor which bridges the two iron atoms, with the proximal Fe atom linked to a 4Fe4S cluster and the site of dihydrogen binding and activation believed to be located on the distal Fe atom. The co-ordination spheres of the two iron atoms are completed by cyanide and carbon monoxide ligands (Fig. 1b). A further type of hydrogenase, H_2-forming methylenetetrahydromethanopterin dehydrogenase (Hmd) does not contain iron–sulfur clusters and, until recently [19], was thought not to contain iron at the active site. Whereas recent studies of Hmd suggest that this hydrogenase also contains carbon monoxide-bound iron at the active site [20] this class of enzyme will not be considered further in this review since vibrational spectra are available only for the native and CO inhibited forms.

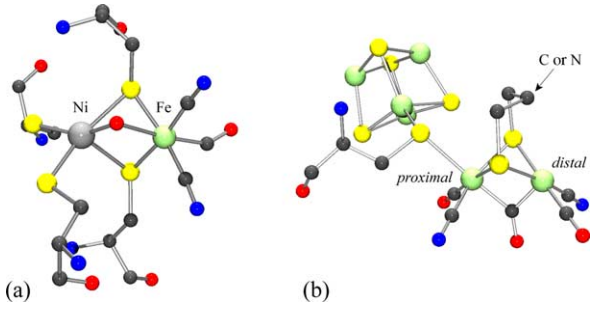

Fig. 1. (a) The Ni–Fe centre of the oxidised, inactive state of the [NiFe]-hydrogenase from *D. gigas* [21] and (b) a composite structure of the H-cluster based on the structures of the [FeFe]-hydrogenases isolated from *C. pasteurianum* [17] and *D. desulfuricans* [18].

The complementary nature of the information available from crystallographic and spectroscopic studies of proteins is well illustrated by investigations into the active sites of the hydrogenases. The mixed carbonyl/cyanide coordination of the Ni–Fe centre being first shown unambiguously by Bagley and Albracht by the use of IR spectroscopy [22–24]. Whereas the application of IR spectroscopy to the study of metal carbonyl complexes is a mature field [25,26], the effectiveness of the approach to metalloenzymes containing metal carbonyl species is amplified by the imprecise characterisation of the molecular details of the active site generally available from protein crystallography. Additionally, the presence of multiple iron sites within the enzymes complicates the analysis of results from techniques such as Mössbauer [27] or EXAFS [28] where the absorptions arising from the different iron atoms are not easily separated.

3. Spectroelectrochemistry (SEC)

The study of systems featuring multiple redox states necessarily requires control of the redox level and this may be achieved by chemical or electrochemical means. The alternate approaches afford particular advantages and suffer from

different limitations. In the case of enzymes, different redox levels can be obtained by reaction with redox partners, substrates or inhibitors. In these cases physiologically relevant states of the system are generated. Electrochemical methods may provide greater control of the redox level but in these cases the rate of oxidation/reduction is generally slow and the identification of the physiologically relevant oxidation states may not be straightforward. The chemical (and biochemical) characteristics of the system and the sampling requirements dictate whether spectroscopic examination of the electrochemically generated product is most appropriately conducted in situ or ex situ. SEC is concerned with the spectroscopic study of in situ electrogenerated products [29–31]. For IR and UV–vis spectroscopy several different approaches have proved to be effective and these may be distinguished in terms of the characteristics of the working electrode. These include (i) optically transparent electrodes, (ii) perforated electrodes and (iii) reflective electrodes. To these may be added approaches in which a probe beam is brought close to the working electrode of an electrosynthesis cell by means of a waveguide or optical fibre. The sampling element may consist either of a pair of launch and collection fibres or include an optical element that is arranged so as to give near total internal reflection (attenuated total reflection, ATR). In the latter case the spectrum of the solution in contact with the ATR crystal is sampled. Detailed discussions of the full range of spectroscopic techniques, together with their physical basis, may be found in various sources [30,32,33]. A discussion of the technical aspects of the experiments will be limited to the techniques used to study hydrogenase or hydrogenase model compounds.

3.1. Optically transparent or perforated electrodes

In optical terms the simplest SEC approach involves the use of transparent electrodes. For visible spectroscopy doped tin oxide affords a useful spectral window [34]. More recently B-doped diamond has been shown to be suitable for UV–vis and IR spectroscopy [35,36]. An alternate strategy is to use a thin gauze as the working electrode and cells constructed using this approach may be used for both UV–vis and IR spectroscopy. In the latter case the path length must be minimised owing to strong solvent absorption. Whereas the principle for construction of the cell is straightforward the implementation can present difficulties. Moss et al. [37] have reported a cell design that is optimised for IR-SEC studies of proteins and cells based on this design have been used for the SEC studies conducted on the [NiFe]-hydrogenase.

A schematic cross-sectional view of the Moss cell is shown in Fig. 2. The working electrode consists of a 6 μm-thick, 70% transparent Au mini-grid and this together with the Pt foil counter and Ag/AgCl reference electrodes complete the three-electrode geometry. An important feature of the cell for applications using proteins is the low sample requirement, where a 3–5 μL drop of solution is sufficient to fill the 20 mm diameter × 15 μm thick space formed by the CaF_2

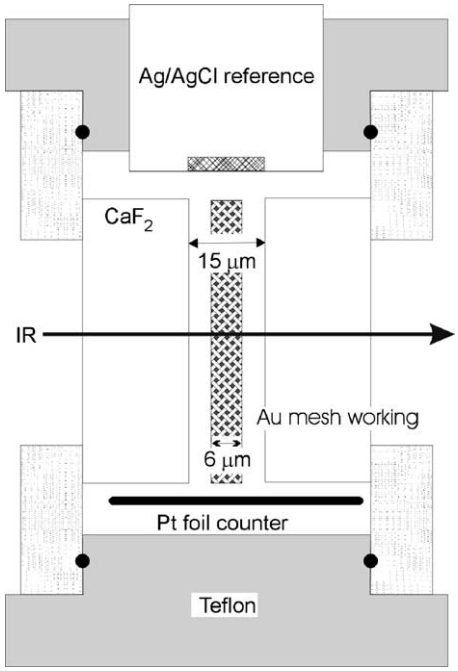

Fig. 2. Cross-sectional view of the transmission IR-SEC cell reported by Moss et al. [37]. For the experiments conducted by de Lacey et al. (e.g. [38]) a 70% transmitting, 6 μm thick, gold mesh was used as the working electrode. Note that the dimensions of the cell are not drawn to scale.

windows. The outer cavity of the cell is filled with buffer/salt solution. Despite the contact between the sample solution and the surrounding medium the rate of dilution was reported to be ∼5% over 24 h [37]. In order to improve the rate of heterogeneous electron transfer and reduce the effects of protein denaturation electrode surface modifiers or electron transfer reagents may be added to the sample solution. Owing to the high electrode surface area to volume ratio the system rapidly equilibrates following a change in applied potential (1–2 min). Although factors such as the IR drop within the cell may lead to an offset to the cell potential, excellent Nernstian concentration/potential plots were obtained for model studies of cytochrome *c* [37].

3.2. Absorption/reflection (RA)-SEC cells

It has been appreciated since the late 1960s that the thin layer of solution trapped between an electrode and a barrier may be subject to spectroscopic investigation provided that the barrier is transparent to the radiation over the energy range of interest and the electrode is sufficiently reflective [39]. Whereas the optical arrangement needed for such experiments is somewhat more complicated than that required for transmission experiments several advantages follow from the adoption of such an approach. These include (i) an effective doubling of the optical path length, (ii) the presentation of a well-defined highly polished electrode surface to the solution, (iii) a reduced average distance between the solute species and the electrode leading to an increased rate of electrosynthesis, (iv) a more flexible range of cell geometries and

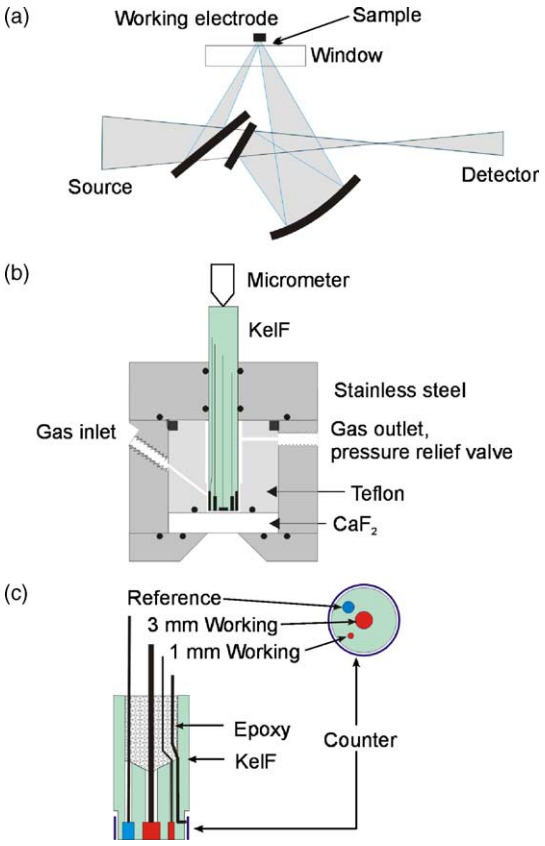

Fig. 3. Schematic diagram of a cell suitable for RA-SEC studies for solutions maintained under elevated gas pressures [41]: (a) optical path (b) cell body and (c) multielectrode assembly.

(v) the possibility of obtaining orientation-selective information through the use of polarised radiation. This approach is favoured in our laboratory, mostly on account of the more rapid rate of electrosynthesis and the fewer constraints placed on the cell geometry.

The basic optical arrangement for RA-SEC cells is shown in Fig. 3a [40]. The working electrode is placed at the focus of the probe beam of the spectrometer and the specularly reflected light is refocused using a spherical or off-axis parabolic mirror and directed onto the detector. For studies conducted on metal carbonyl compounds, where CO association or dissociation reactions may accompany a change of redox state, it is advantageous to be able to change the concentration of gaseous species; that is to conduct the experiments at various gas pressures. A simple RA-SEC cell capable of operation under elevated gas pressures has been reported [41] and this involves the use of a Teflon sample holder located within a stainless steel casing (Fig. 3b). Standard Swagelok^{TM} fittings are used to connect the cell to a gas line. The working electrode consists of a 3 mm diameter disc of an appropriate material. It is noteworthy that the reflectance of vitreous carbon, while lower than that of platinum, is sufficient to permit its use in IR-SEC experiments. This is particularly important for studies that involve dihydrogen. While it is possible to incorporate a more conventional reference electrode into the cell design it is generally not possible to obtain a close placement between the working and reference electrodes. This problem may be alleviated somewhat by the use of a silver pseudo-reference electrode which also contacts the thin layer of solution trapped between the electrode assembly and the IR transmitting window. While the potential of this reference will clearly be subject to drift, over the timeframe of the SEC experiments this is rarely found to present significant problems. Incorporation of an additional 1 mm diameter working electrode into the multielectrode assembly (Fig. 3c) allows electrochemical characterisation of the solution and this can be used to estimate the potential of the reference electrode. The solution volume required for operation depends on the shape of the Teflon liner contained within the cell. For the cell design shown in Fig. 3, a solution volume of ∼70 μL is sufficient when using non-volatile solvents. Since the solution actually subject to electrosynthesis in an individual experiment is small, ∼0.1 μL, a number of separate experiments can be conducted on the same solution provided that the surface of the electrode is not contaminated.

3.3. In situ sampling of bulk electrosynthesis experiments

Optical waveguides provide a convenient means of collecting spectroscopic information from more conventional electrosynthetic cells. For the IR region of the spectrum chalcogenide glasses provide a satisfactory performance over a reasonably broad spectroscopic window (900–4000 cm^{-1} with an opaque region around 2190 cm^{-1}) and sampling is most conveniently performed using an ATR probe [42]. In this arrangement the IR radiation is internally reflected within an IR transparent crystal of high refractive index and the IR spectrum is obtained through the interaction between the sample and the non-propagating evanescent wave that decays exponentially out from the crystal at the point of internal reflectance. The penetration depth of the evanescent wave depends on the difference in refractive indices of the two media, the wavelength of the radiation and the angle of incidence of the radiation within the crystal. A penetration depth of ∼1 μm would be obtained for a Ge element with 1000 cm^{-1} radiation in absorbing media [32]. In order to increase the sensitivity of these probes it is necessary to use optical configurations with multiple reflections and a ReactIR^{TM} instrument with a 30-bounce Si probe (SiCOMP) has recently been used to identify the products formed during the bulk electrolysis of bis-thiolate bridged diiron compounds [43].

This approach is suited to cases when the electrogenerated products are stable over the duration of the electrosynthesis where, depending on the volume of the solution, times range from minutes to hours. Once the solution is in a spectroscopically well-defined state then a range of electrochemical and spectroscopic measurements may be conducted on the product. A variation of this approach involves coating the ATR element with a metallic conductor that is sufficiently thin to allow penetration of the evanescent wave into the solution

[32]. The metallic conductor then serves as the working electrode and only the solution within ~1 μm of the ATR element is examined. While this approach would appear to provide the rapid rate of electrosynthesis provided by the thin film geometries with more conventional electrode geometry, the high resistance of the thin working electrode and the limited effective spectral range combine to limit the impact of this approach.

4. SEC studies of [NiFe]-hydrogenase enzymes

The vital role that EPR spectroscopy has played in the development of an understanding of the chemistry of the [NiFe]-hydrogenases is well documented [44–51] and will not be further developed in this review. Three EPR-active states of the enzyme, designated Ni-A, Ni-B and Ni-C [45,52–54], have provided fixed points for the collection and analysis of a range of chemical and physical measurements of the enzyme. Briefly, these states correspond to the oxidised, inactive forms of the enzyme (Ni-A and Ni-B) and a reduced active form (Ni-C). Activation of the enzyme, often by incubation of the enzyme under H_2, proceeds very slowly from Ni-A but much more rapidly from Ni-B and accordingly the Ni-A and Ni-B states are often termed unready and ready, respectively. The potential and pH dependence of the different species have been defined by EPR experiments [55–57]. The early reports of IR spectroscopy of the [NiFe]-hydrogenase from *Chromatium vinosum* [23] and *Desulfovibrio gigas* [16] between 1900 and 2150 cm^{-1} revealed beautifully simple spectra with a more intense band at lower wavenumber due to the ν(CO) mode and a pair of higher wavenumber bands due to the ν(CN) modes [24]. In addition to providing an unambiguous identification of the diatomic ligands bound to the iron atom, IR spectra can be obtained from both the EPR active and silent states of the enzyme. This is well illustrated by the IR-SEC experiment shown in Fig. 4 where reduction of Ni-B gives four product states of which only Ni-C is EPR active [38]. Whereas the interpretation of IR spectra is often complicated, cyanide and carbonyl groups can generally be treated as local oscillators and the frequencies of the ν(CO) and ν(CN) modes provide a good measure of the electron richness of the metal atom to which they are bound. For the dicyanides, the angle between the CN groups can be estimated from the relative intensities of the two ν(CN) bands [58]. The IR spectra themselves are remarkably well defined, with the half-widths of the bands often limited by the resolution of the spectrometer, reminiscent of the spectra obtained from metal carbonyl species isolated in noble gas matrices [25]. The Ni–Fe centre, being deeply buried within the protein [21], is a beautiful example of a matrix isolated active catalyst.

The initial IR-SEC study of the [NiFe]-hydrogenase from *D. gigas* has established the framework on which the subsequent studies are built [38]. The experiments were conducted using the Moss transmission SEC cell (Fig. 2) on a small quantity of enzyme solution (1–2 mM, 10 μL) containing Tris buffer (100 mM), KCl (100 mM) and a mixture of redox mediators [38]. A summary of the inter-conversions between the enzyme states is given in Table 1 and a set of spectra obtained from one set of experiments is shown in Fig. 4.

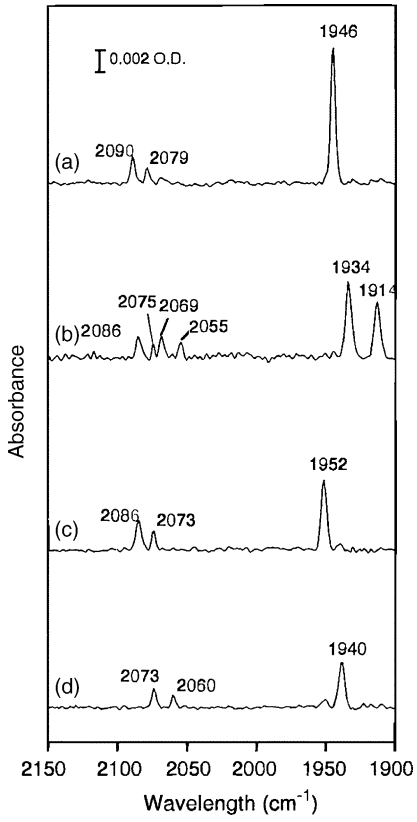

Fig. 4. IR-SEC spectra obtained by reduction of the Ni-B form of the hydrogenase from *D. gigas*: (a) Ni-B, (b) a mixture of Ni-SI_I and Ni-SI_{II}, (c) Ni-C and (d) Ni-R. Reprinted with permission from [38]. Copyright 1997 American Chemical Society.

Aerobic isolation of the enzyme provides the sample in the Ni-A state with a structure corresponding to that given in Fig. 1a. Chemical conversion into the inactive, ready Ni-B and activated Ni-C states is well known as are the EPR spectra characteristics of these states. One procedure for chemical conversion between the different enzyme states is given in Table 1 and the IR spectra of these chemically generated states have been reported [16]. The IR spectra of chemically and electrochemically generated samples of the enzyme in different states are indistinguishable and this suggests that the integrity of the sample is maintained in the IR-SEC experiment. This is also reflected by the excellent agreement for the potential dependence of the concentrations of the Ni-B and Ni-C states obtained by EPR and IR spectroscopy [50,57,59].

The potential dependence of the relative concentrations of the oxidised and reduced species involved in the redox couple depends on the number of electrons involved in the reaction and this is given by the Nernst equation. A plot showing the potential dependence of the concentrations of the Ni-B, Ni-SI, Ni-C and Ni-R states of the activated enzyme as determined by IR-SEC experiments is shown in Fig. 5. Analo-

Table 1
Chemical and electrochemical inter-conversions between the IR-characterised enzyme states of *D. gigas*

Electrochemical[a]	State[b]	ν(C{O/N})[c] (cm^{-1})	Chemical[d]
-210	Ni-A*	1947, 2083, 2093	dithionite 4° C
	Ni-SU	1950, 2089, 2099	
	Ni-B*	1946, 2079, 2090	O_2, fast
-135	Ni-SI_I	1914, 2055, 2069	H_2 40° C 2 h; O_2
slow -500	Ni-SI_{II}	1934, 2075, 2086	
-365	Ni-C*	1952, 2073, 2086	O_2, slow
-430	Ni-R	1940, 2060, 2073	1% H_2

[a] Redox potentials are given in mV with respect to NHE at a pH of 7.7. Double-headed arrows are used the reduction potentials correspond to the midpoint potential for the couple, E'_m, at 40 °C.
[b] The designation of the state is adapted from that given in [38]. An asterisk is used to designate the EPR active states of the enzyme. The two different forms of Ni-SI, Ni-SI_I and Ni-SI_{II}, differ in terms of their level of protonation.
[c] Values are taken from electrochemically [38] or chemically reduced [22] enzyme. The IR spectra of the electrochemically or chemically generated samples are indistinguishable.
[d] The example given follows the procedure given in [16].

gous results for the Ni-A/Ni-SU couple reveal a well-defined Nernstian response, consistent with its assignment to a one-electron process. It was noted that there was some deviation from Nernstian behaviour for the Ni-C/Ni-R couple and this was attributed to the effects of H_2 production as a result of catalytic activity of the hydrogenase [38]. The pH dependence of the midpoint potential for the couple (E'_m) provides a quantitative measure of the number of protons involved in the reaction, where at 40 °C a slope of −62 mV/pH unit would correspond to a process that consumes one proton per electron. The measured slopes for the corresponding plots for the Ni-A/Ni-SU, Ni-B/Ni-SI, Ni-SI/Ni-C and Ni-C/Ni-R couples were found to be −55, −36, −47 and −43 mV, respectively. Since the couples involving Ni-SI are complicated by a proton equilibrium a composite value is measured and this accounts for the observed slopes. As already noted measurements of the Ni-C/Ni-R couple are complicated by evolution of H_2 and the E'_m/pH slope of −43 mV/pH unit was interpreted as involving a one-electron, one proton reaction. These experiments provide a remarkably clear picture of the different electron/proton levels of the enzyme.

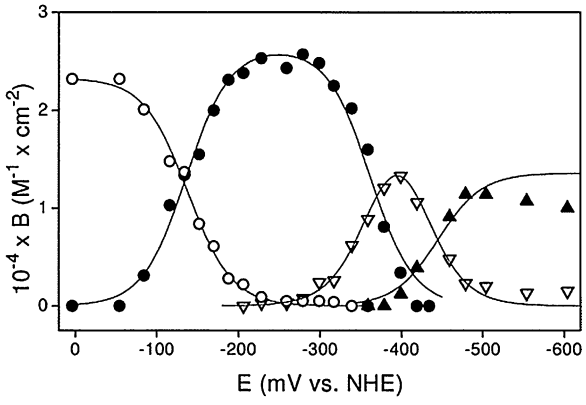

Fig. 5. Potentiometric titration of the redox states of the activated hydrogenase from *D. gigas*: (open circles) Ni-B (1946 cm^{-1}); (filled circles) Ni-SI_I and Ni-SI_{II} (1914 + 1934 cm^{-1}); (open triangles) Ni-C (1952 cm^{-1}); (filled triangles) Ni-R (1940 cm^{-1}). The solid lines are the best-fits for one-electron Nernstian processes. Reprinted with permission from [38]. Copyright 1997 American Chemical Society.

Detailed IR-SEC studies have more recently been reported for [NiFe]-hydrogenases obtained from *D. fructosovorans* [60,61] and *Allochromatium vinosum* [62] and these provide important insights into the activation/inactivation processes and CO inhibition. There is a remarkable similarity between the stable potential ranges of the different states of hydrogenases sourced from different organisms, including examples of both periplasmic and membrane-bound enzymes. This is also reflected by highly concordant IR spectra obtained for the different states. Differences in sample preparation may also lead to additional states; "as-isolated" preparations of *A. vinosum* contains a variable amount of an additional state with a ν(CO) band at 1909 cm^{-1} and this was attributed to an undefined sulfur species bridging the Ni and Fe sites. Whereas activation of the enzyme in this state was found to be very slow, once activated the inter-conversions between the different states of the enzyme are almost identical to those found for *D. gigas* [62].

Whereas the presence of a bridging ligand at the Ni–Fe site in the different hydrogenase states is more clearly established by EPR spectroscopy [63,64] and X-ray crystallography [21,65], the rate of activation/inactivation of the enzyme is most easily followed by IR spectroscopy. The recent IR-SEC studies on the hydrogenases from *D. fructosovorans* and *A. vinosum* examined the effect of pH, solvent isotopic substitution and site-directed mutagenesis on the rate of activation/inactivation [60,62]. Primary kinetic isotope effects were found for the oxidation of Ni-SI to Ni-B but not for the reduction of Ni-A to Ni-SU (although the rate constants were determined with less reliability owing to overlap of the ν(CO) bands) [60]. Interestingly, the rate of oxidation of Ni-SI is reported to be independent of pH for *D. fructosovorans* but not for *A. vinosum* [66]. The E25Q mutant of *D. fructosovorans* (replacement of the glutamic acid residue by glutamine) was examined in order to test the proposition that hydrogen bonding involving Glu25 (Glu18 in *D. gigas*) is the major difference between the Ni-A and Ni-B states [67]; in the former case there is a hydrogen bond between Glu25 and a nickel-bound cysteine residue, in the latter case the thiolate is protonated. The E25Q mutation impairs rapid proton transport from the active site but does not prevent the formation of the active states of the enzyme (as identified by their IR spectra) and this is consistent with the retention of catalytic activity for *ortho*-H_2/*para*-H_2 inter-conversion.

The rate of activation of the mutant was slightly reduced (1.25 times) but the rate of anaerobic inactivation was significantly slower (six times) [60]. While this is consistent with Glu25 having a role in incorporation of the bridging oxygen ligand into the active site it is less clear whether this residue plays a more central role in defining the Ni-A and Ni-B states. It is noted that there is reference to crystallographic evidence for the difference between Ni-A and Ni-B to be the identity of the bridging ligand, where in the former case a diatomic ligand, most likely a species derived from dioxygen, is implicated [62]. A manuscript detailing the crystallographic basis for this suggestion has been submitted for publication (Ref. [44] of [62] and Ref. [49] of [68]).

The relationship between the different states of [NiFe]-hydrogenase is given in Scheme 1 and this is based on studies of both periplasmic [38,60,61] and membrane-bound [62] enzyme. The IR-SEC studies have resulted in a marked expansion in the number of states, particularly (although not exclusively) those that are EPR-silent. The distinction between the Ni-SI_I and Ni-SI_{II} states has been attributed to protonation and dissociation of the bridging hydroxyl group. At the lower temperatures used for the study of *A. vinosum* [62] it was possible to distinguish, on the basis of reactivity, between "ready" and "active" forms of Ni-SI_{II}. The difference was interpreted in terms of a blocking of the active site by the dissociated water molecule. The two different forms of Ni-C have been attributed to different redox states of the nearest (proximal) iron–sulfur cluster. This interpretation is supported by analysis the low temperature EPR spectra in terms of spin–spin interaction between the Ni centre and the proximal iron–sulfur cluster [71]. The forms of Ni-C with ν(CO) of 1950 and 1948 cm^{-1} (*A. vinosum*) correspond to the oxidised and reduced forms of the proximal iron–sulfur cluster, respectively [62]. Several distinct Ni-R states have also been identified with relative populations that are pH dependent. This, together with the moderately large difference in ν(CO) associated with the Ni-R states (8–15 cm^{-1}), suggest that they are related by a difference in protonation of the active site [62].

Carbon monoxide is a competitive inhibitor of [NiFe]-hydrogenases and IR-SEC studies of CO-saturated solutions of the enzyme have permitted the identification of the enzyme states that react with CO and provided insights into mode and site of CO binding [61]. More recently stopped-flow (SF) FT-IR studies of CO binding to *A. vinosum* have provided more detailed insights into the dynamics of these reactions [70]. The Ni-A, Ni-B and Ni-SU states of the hydrogenase from *D. fructosovorans* are unreactive with CO whereas the Ni-C and Ni-SI states evolve to give products that feature additional IR bands due to the extrinsic CO. The initial suggestion that Ni-R is also unreactive with CO [61] must be revised in light of the subsequent SF-FT-IR studies [70].

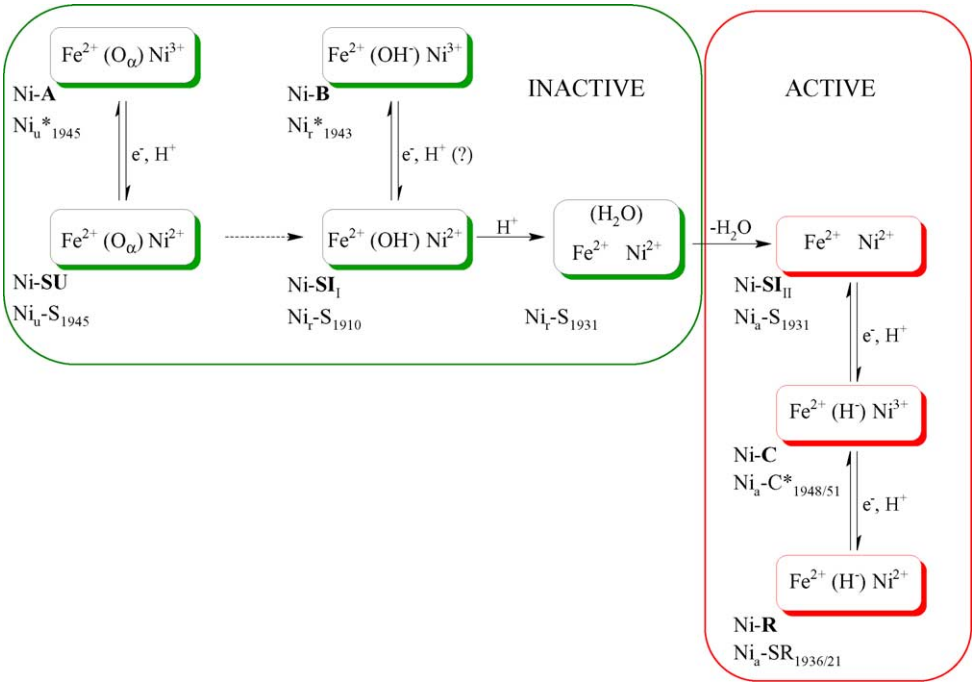

Scheme 1. Overview of the different states of the Ni–Fe site of [NiFe]-hydrogenase. The nomenclature is based on that initially adopted to designate the EPR active states (Ni-A, etc.) although it is common to omit the "Ni" as, for example, in [38]. The nomenclature adopted by Albracht and co-workers [62,69,70] is also given, where the subscript on the Ni distinguishes between the unready, ready and active forms of the enzyme, the "S" designates an EPR silent state and the number subscript indicates the wavenumber of the ν(CO) mode. The bridging ligand, O_α, is most commonly taken to be OH^-, but has recently been suggested to be a diatomic ligand (most likely derived from dioxygen) [62]. There are multiple forms of Ni-C and Ni-R and these have been suggested to differ in terms of the redox state of the nearest (proximal) iron–sulfur cluster and/or protonation of the cysteinyl sulfur atoms. A more detailed description of the different states, including the redox levels of the iron–sulfur clusters has recently been published [69,70].

The insensitivity of the Ni-A and Ni-B states to CO can readily be understood in terms of the high oxidation state of the Ni centre (Scheme 1). The oxidation-state dependence of CO binding to sulfur-bound nickel complexes is demonstrated by IR-SEC studies of $[Ni(mnt)_2]^{2-}$, where mnt = maleonitrile-1,2-dithiolate, under elevated CO pressures. There is no evidence for CO binding until reduction to the trianion (which corresponds to a formal Ni^{I} species) [41]. Re-oxidation to the dianion leads to dissociation of the CO ligands. It should be noted that owing to differences between the thiolate and dithiolene ligands the oxidation state required for CO binding does not transfer directly from the mnt complex to the enzyme. Further studies of the redox state dependence of CO binding to more relevant nickel thiolate complexes would be useful since they would provide a context for the interpretation of the CO binding to different states of [NiFe]-hydrogenases.

Accessability to the active site may, in addition to the reduction level, control CO binding and this is evident from the observation that both Ni-SU and Ni-R states are unreactive with CO. The ligand bridging the Ni and Fe centres of Ni-SU (Scheme 1) is slowly displaced and this ligand blocks co-ordination of CO (and H_2). The CO-inhibited Ni-SI state, SI-CO, formed by addition of CO to Ni-SI has an additional $\nu(CO_{ext})$ band at 2055 cm^{-1}, where the assignment of the band to extrinsic CO was confirmed by ^{13}CO substitution [61]. Based on the high wavenumber of the $\nu(CO_{ext})$ band it can be concluded that the CO ligand does not occupy a bridging position between the Ni and Fe centres. Moreover, the insensitivity of the intrinsic ν(CO) and ν(CN) modes to CO binding, indicate that the extrinsic CO group cannot be bound to the $Fe(CN)_2(CO)$ subunit, i.e. that CO is bound to the nickel atom. Since the intrinsic CO ligand of the Ni–Fe centre does not undergo exchange at a significant rate following exposure of the enzyme to ^{13}CO, even under reducing conditions, either the $Fe(CO)(CN)_2$ unit must remain inert through all of the accessible redox states of the enzyme or that the protein blocks access of CO to the Fe site.

The conclusion that the extrinsic CO group is terminally bound to the Ni centre is confirmed by a series of high-resolution (1.2–1.4 Å) structures from crystals of CO-inhibited [NiFe]-hydrogenase from *Desulvibrio vulgaris* Miyazaki F (Fig. 6) [72]. A surprisingly large range of Ni–C–O angles were obtained (136.2–160.9°) and this was taken to suggest the presence of several CO co-ordination geometries and this is consistent with the weak Ni–CO binding. XAFS experiments on the [NiFe]-hydrogenase from *C. vinosum* have previously been interpreted in terms of a linear Ni–C–O moiety [73]. The high wavenumber of the ν(CO) mode of extrinsic CO matches with the low wavenumber of the ν(NiC) mode obtained from resonance Raman spectroscopy and this is consistent with weak π backbonding to the CO group, as would be expected given the relatively high oxidation state of the Ni atom.

Reduction of SI-CO results in the formation of a further reduced species $(SI\text{-}CO)_{red}$ where potentiometric titrations

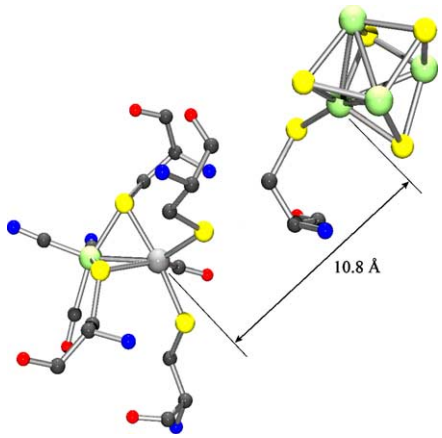

Fig. 6. The Ni–Fe centre and proximal 4Fe4S cluster of the Ni-CO state of the hydrogenase from *Desulvibrio vulgaris* Miyazaki F [72]. The three diatomic ligands were refined as CO and the designation of one of these ligands as CO and CN is arbitrary. The closest Ni–Fe(4Fe4S) distance is shown.

show that the $SI\text{-}CO/(SI\text{-}CO)_{red}$ couple be a single electron process [61]. The shift of the ν(CN) and the ν(CO) bands of both extrinsic and intrinsic CO on reduction is of a similar magnitude (1–3 cm^{-1}) and to lower wavenumber. The small frequency shift of the ν(CO) and ν(CN) modes is explained in terms of the redox process being based on the proximal iron–sulfur cluster (Scheme 2). The changes observed in the UV–vis spectra are consistent with this interpretation [61].

The binding of CO to the formal Ni^{III} centre of Ni-C would, at first sight, appear unlikely particularly given the high value of ν(CO) for the adjoined $Fe(CO)(CN)_2$ fragment. Since binding of CO can be coupled to reduction of the nickel centre by the proximal iron–sulfur cluster it is understandable that the equilibrium should lie in favour of the carbonylated product. It is noted that the rate of reaction with CO is more rapid for both Ni-SI and Ni-R than for Ni-C [70]. While the binding of CO to the formal Ni^{II} centre may be understood in terms of its thiolate-rich co-ordination environment it is nonetheless surprising that addition of the π-acid ligand CO does not make accessible lower oxidation states of the metal

The elegant series of IR-SEC experiments conducted by de Lacey, Fernandez and co-workers demonstrate very beautifully the central role of IR spectroscopy in establishing the connections between the many different states of the [NiFe]-hydrogenases. This is possible for two main reasons; first, all the accessible states of the enzyme are observable with approximately equal ease, and second, the very simple pattern of well resolved bands due to ν(CO) and ν(CN) provide clear, unambiguous and quantifiable identification of the states. The combination of electrochemical and spectroscopic techniques then allows determination of the number of electrons, and protons, of the redox transformations. Onto this framework can be assembled the models of the chemistry elaborated by the broadest range of chemical, biochemical, physical and theoretical techniques.

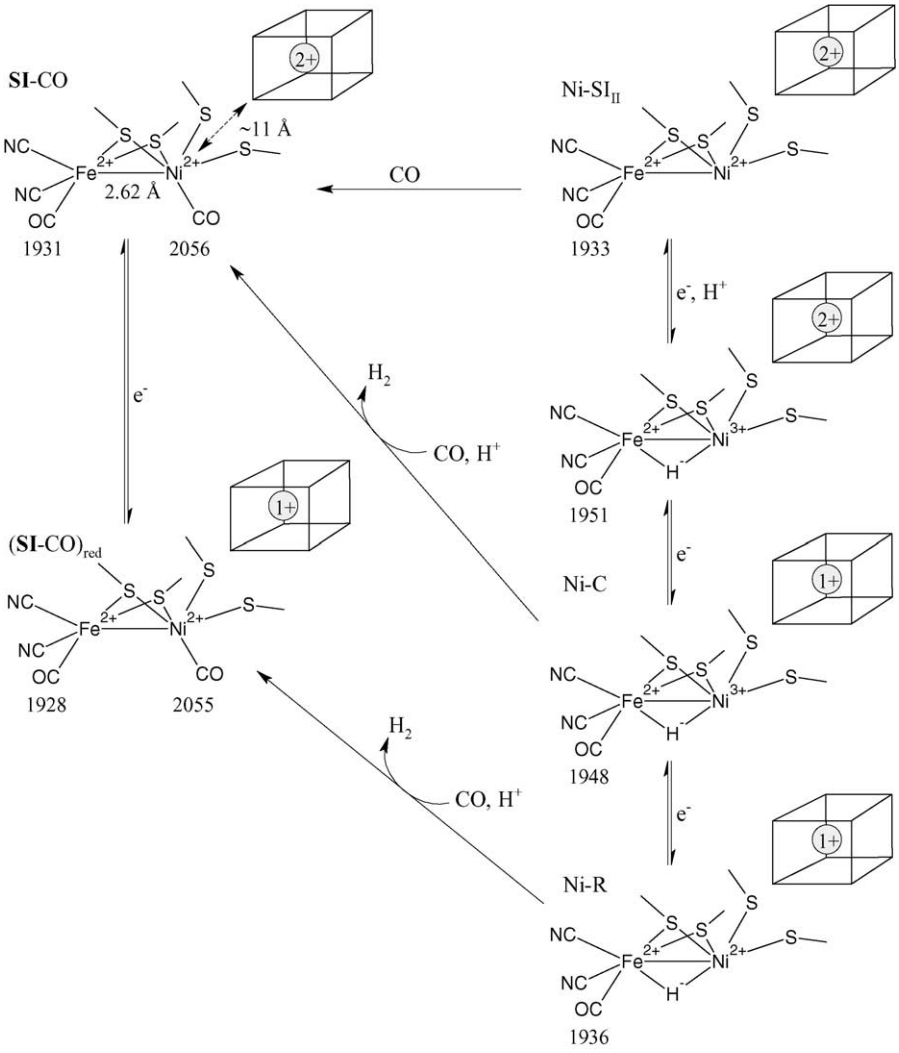

Scheme 2. Formation of CO bound states of the Ni–Fe centre based on studies of the hydrogenase from *D. fructosovorans* [61] and *A. vinosum* [70]. The wavenumbers of the ν(CO) bands are given below the relevant groups. Reaction between CO and Ni-R has only been shown for the hydrogenase from *A. vinosum*. The proximal iron–sulfur and Ni–Fe centres are shown where the charge indicated corresponds to the naked 4Fe4S cube. The relative positions of the CO and CN^- groups of the $Fe(CO)(CN)_2$ fragment is arbitrary.

5. SEC studies of [NiFe]-hydrogenase model compounds

Progress towards the isolation of compounds that are structural models of the Ni–Fe site (and H-cluster) has been reviewed [14,74] and is discussed in another contribution to this issue [75]. In contrast to the extensive SEC studies conducted on the [NiFe]-hydrogenase enzymes, the model compounds so far identified have not yielded to similar analysis. Hydrogenase activity has been reported for a number of complexes that, within the inclusive definition of the literature, are considered to be [NiFe]-hydrogenase model compounds.

Prior to the determination of the structure of the Ni-Fe active site Thorp and co-workers reported electrocatalytic proton reduction by the nickel(II) macrocyclic complex, M_I [76]. While it is clear that the compound is not structurally related to the enzyme this example gives an indication of the generality of proton reduction/dihydrogen oxidation catalysis at a nickel centre. In aqueous solution two catalytic waves are observed with E_p values of ~−0.9 and ~−1.1 V (versus SCE). While the electrocatalytic current is not particularly large the onset potential for proton reduction is comparable to that of diiron carbonyl compounds considered in Section 8.

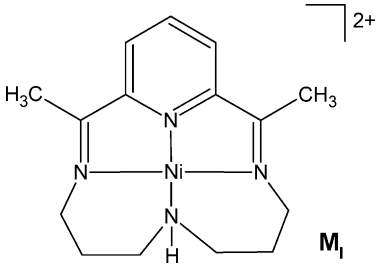

M_I

An elegant example of heterolytic dihydrogen cleavage has been reported by DuBois and co-workers and this involves

a bis bidentate phosphine complex of Ni^{II} where the bidentate phosphine ligand includes a basic nitrogen atom, M_{II} [77]. The juxtaposition of the proton and hydride acceptor sites within the molecule increases the rate of proton exchange of the nickel hydride and, most likely, hydrogen activation. The free energy calculated for the heterolytic cleavage of dihydrogen for related Ni^{II} phosphine complexes appears to be related to the tetrahedral distortion of the co-ordination geometry, where a larger distortion lowers the energy of the acceptor orbital for the hydride ligand.

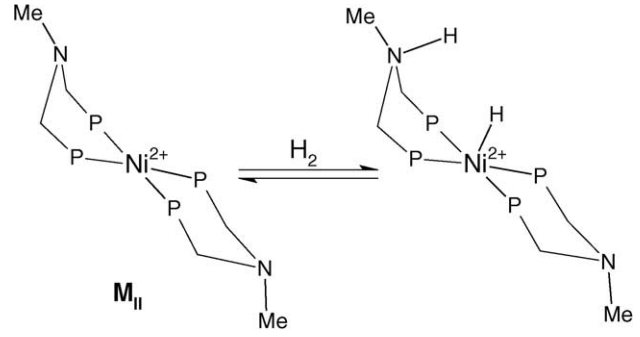

It is noted that the tetrahedrally distorted $Ni^{II}S4$ complex reported by Prakash and co-workers, M_{III}, also catalyses HD exchange, albeit slowly at room temperature [78]. The mechanism for the reaction is proposed to proceed by heterolytic cleavage of dihydrogen with protonation of one of the dithiolene sulfur atoms and formation of a nickel hydride.

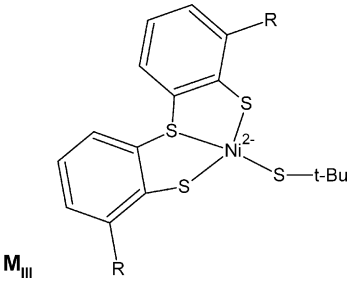

Two recent examples of trinuclear clusters are of interest both in terms of their spectroscopic and chemical behaviour. Schröder and co-workers have reported the synthesis and spectroscopy of a $Ni^{II}S4$ complex which bridges the iron atoms of a $Fe_2(CO)_6$ unit (M_{IV}) [79]. While the formal oxidation states of the Ni^{2+} and Fe^0 atoms are low, the wavenumbers of the ν(CO) modes are high (2035–1955 cm^{-1}). Following reduction the ν(CO) bands shift lower by 66–73 cm^{-1}. Analysis of the EPR spectra, supported by DFT calculations, indicates that the singly occupied molecular orbital is ~24% localised on the Ni atom. A final example, from the Sellmann laboratory, features a 2NiFe complex (M_V) [80]. Three quasi-reversible redox processes are observed with $E_{1/2}$ values of −1.071, −0.095 and 0.844 V (versus NHE). Protonation of the neutral complex results in a shift of the ν(CO) band from 1916 to 1976 cm^{-1}, and this together with the observation of an EPR spectrum suggests that protonation leads to oxidation of the complex together with dihydrogen formation. This conclusion is supported by the observation that the IR and EPR spectra of the product obtained following protonation match that formed by one-electron oxidation of the neutral compound by ferrocenium.

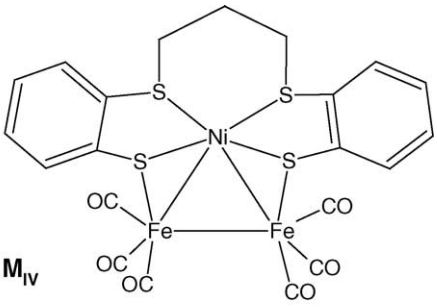

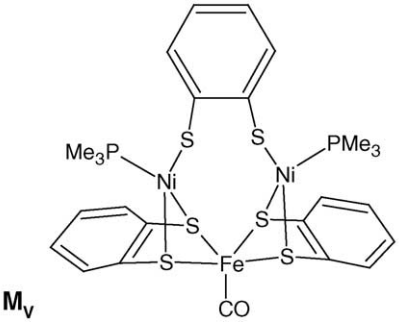

6. SEC studies of [FeFe]-hydrogenase enzymes

As for the [NiFe]-hydrogenases IR spectroscopy has played a central role in the characterisation of the H-cluster of the [FeFe]-hydrogenases, although in this instance fewer redox levels of the enzyme have been identified. The first high quality IR spectra from an [FeFe]-hydrogenase was reported by Albracht and co-workers from enzyme derived from *Desulvibrio vulgaris* (Hindenborough strain) [81]. Whereas the air isolated form gives a relatively simple spectrum, reduction by dihydrogen results in a complicated spectrum suggesting the generation of a mixture of products. The spectra were simplified by the replacement of dihydrogen by CO, to give a CO-inhibited form of the enzyme, or argon. These measurements revealed a single low wavenumber ν(CO) mode for both the oxidised and CO-inhibited forms and this was interpreted in terms of a bridging CO group. This conclusion was later confirmed by the report of the X-ray structures [17,82].

IR-SEC studies conducted using a Moss cell on [FeFe]-hydrogenase isolated from *D. desulfuricans* demonstrate the electrochemical activation of the enzyme. The aerobic isolated enzyme is converted to the reduced form by application of a potential of −535 mV (versus NHE) and the oxidised active form, H_{ox}, is obtained by reoxidation at −285 mV (Fig. 7) [82]. Analogous experiments conducted on solutions satu-

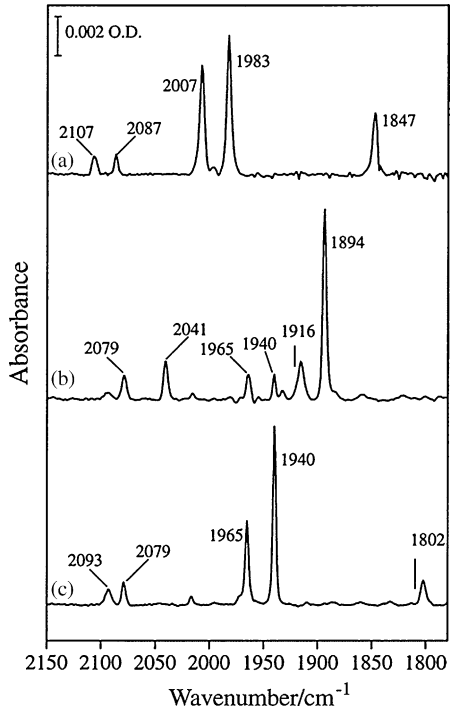

Fig. 7. IR-SEC measurements from 1 mM solutions of the [FeFe]-hydrogenase from *D. desulfuricans* showing (a) the aerobuc isolated enzyme, (b) the reduced form, H_{red} (−535 mV) and (c) the active oxidised form, H_{ox}, obtained by oxidation of H_{red} at −285 mV. Reprinted with permission from [82]. Copyright 2001 American Chemical Society.

rated with CO give the CO inhibited form of the enzyme, H_{ox}-CO [83]. The crystal structure of the CO-inhibited form of the [FeFe]-hydrogenase from *Clostridium pasteurianum* shows that extrinsic CO binding occurs at the open co-ordination site of the distal Fe atom (Fig. 1b) [84]. The EPR spectra of H_{ox} and H_{ox}-CO forms are well known, giving the "rhombic 2.10" and "axial 2.07" signals, respectively [1].

The IR spectra of H_{ox}-CO and its ^{13}CO substituted analogue have been examined for both chemically [85] and electrochemically [83] generated samples. Neither the ν(CN) nor the ν(CO) mode of the bridging CO group give a measurable change in frequency following ^{13}CO substitution. Of the three ν(CO) modes due to terminally bound CO, one (1963 cm^{-1}) is insensitive to isotopic substitution and the remaining bands shift by 21 and 23 cm^{-1}, about half that expected for a single uncoupled CO oscillator. The magnitude of the shift on isotopic substitution together with the number of CO bands observed in the ^{13}CO experiments require that there be a single non-exchangeable site of extrinsic CO binding where there is coupling with only one of the intrinsic CO groups. This was assigned to the terminal CO group bound to the same (distal) Fe atom [83].

Low temperature photolysis experiments of H_{ox}-CO show the presence of two products; one, which decays at temperatures above 80 K, involves the loss of the bridging ligand and the other, which decays at temperatures above 150 K, has an IR spectrum identical to H_{ox} [85]. Together with X-ray experiments conducted from crystals in the H_{ox}-CO form under photolysis conditions [84,86], these studies provide a structural basis for the analysis of the EPR spectra obtained from similarly prepared samples.

7. SEC studies of [FeFe]-hydrogenase model compounds

The diiron subsite of the H-cluster of the [FeFe]-hydrogenase enzyme has proved to be a far more accessible synthetic target than the Ni-Fe centre of the [NiFe]-hydrogenases [14,87,88]. Structural analogues have been developed from the $Fe_2(\mu\text{-}SR)_2(CO)_6$ compounds first prepared by Reihlen et al. [89] While the mixed carbonyl/cyanide co-ordination of the thiolate-bridged diiron core was unprecedented prior to the revelation of the H-cluster structure, this has proved to be accessible synthetically [90–97]. Whereas much of the work has concentrated on compounds having a pdt bridge, Rauchfuss and co-workers have developed an elegant procedure for the preparation of complexes with a bridging dta ligand [98]. Incorporation of a pendant thioether group into the dithiolate bridge leads to compounds having a {2Fe3S} core with two bridging and one terminal sulfur atom. Modifications of this sort have been reported for both pdt [95] and dta bridging groups [99]. The model compounds are useful in terms of the insights they bring to the chemistry of the catalytic centre during turnover. In this context it is important to develop an understanding of the changes in structure and reactivity that accompany a change in redox state.

Despite the apparent simplicity of the thiolate-bridged diiron hexacarbonyl compounds, $Fe_2(\mu\text{-}SR)_2(CO)_6$, there has been conjecture over the assignment of the number of electrons involved in the reduction process. The initial reports for a range of bis-thiolate and dithiolate bridges suggested a single two-electron process [100]. This interpretation is in keeping with the well-defined redox behaviour of the phosphido-bridged analogues [101,102], and is further supported by recent study of benzene-1,2-dithiolate (possibly extending to benzene-1,2-dimethanethiolate) bridged diiron hexacarbonyl compounds [103]. In this case, reduction has been shown to proceed by a net two-electron process which is comprised of two one-electron steps, where the second reduction occurs at potential more positive than the first. Nevertheless, the electrochemistry of the pdt and bis-thiolate bridged compounds have been shown to have characteristics more in keeping with that expected for a one-electron process [43,104]. Although the basis for the assignment of the process was not discussed, the recent report of the substituted dta [$(SCH_2)_2N$(*p*-bromobenzyl)] bridged diiron hexacarbonyl compound is also suggested to undergo one-electron reduction [105].

Confirmation of the one-electron character of the reduction of $Fe_2(\mu\text{-pdt})(CO)_6$, M_{VI}, follows from the characterisation of the one-electron reduced product. SEC experiments using the cell described in Section 3.2 demonstrate that reduc-

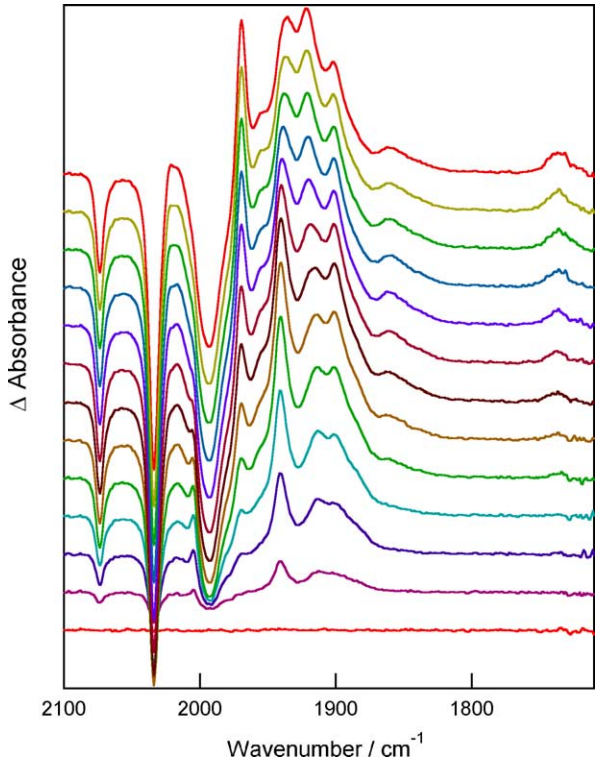

Fig. 8. IR-SEC spectra recorded during reduction of a 5 mM solution of M_{VI} in THF. The time between spectra is 1.4 s. The negative bands correspond to the depletion of the starting material. The figure is based on spectra reported in [104].

tion of THF or CH_3CN solutions of M_{VI} saturated with CO proceeds through a short-lived intermediate, $M_{VI\text{-}A}$, to give a single product, $M_{VI\text{-}B}$, in near quantitative yield (Fig. 8) [104]. The final product, $M_{VI\text{-}B}$, features a bridging CO ligand and coulometry shows the product to be two-electron reduced from M_{VI} (Scheme 3). The observations that $M_{VI\text{-}B}$ is EPR silent and the absence of broadening of its NMR spectra, are consistent with a diamagnetic ground state.

The assignment of $M_{VI\text{-}A}$ to $[Fe_2(\mu\text{-pdt})(CO)_6]^-$ was based on a combination of spectroscopic (IR, UV–vis and EPR) and chemical experiments. In the absence of an external reducing agent the decay of $M_{VI\text{-}A}$ to $M_{VI\text{-}B}$ must be accompanied by its oxidation in a disproportionation-type reaction. This reaction may be examined during SEC experiments by switching the potentiostat to open circuit at a time during the reaction when there is a significant concentration of $M_{VI\text{-}A}$. Experiments of this type show that the $M_{VI\text{-}A}$ decays with a half-life of ~10 s to give both $M_{VI\text{-}B}$ and M_{VI} as is required if $M_{VI\text{-}A}$ is in an intermediate oxidation state [104].

SEC experiments conducted on the related compound $Fe_2(\mu\text{-SEt})_2(CO)_6$ have also been interpreted in terms of a one-electron reduction chemistry [43]. In this case a bulk electrosynthesis cell was used and the solution monitored using a ReactIR™ system with SiCOMP probe. Bulk electrolysis of a CO-saturated CH_3CN solution of $Fe_2(\mu\text{-SEt})_2(CO)_6$ in the 50 mL cell required 4 h and during this time the IR spectra indicated the conversion of the starting material to give a new product. The catholyte was examined by EPR and at 10 K an axial signal was observed ($g_{||} = 1.994$ and $g_{\perp} = 2.117$). Coulometry from these solutions indicated the consumption of ~0.95 electrons per complex. Whereas the results obtained for both $Fe_2(\mu\text{-SEt})_2(CO)_6$ and M_{VI} are concordant, at least in terms of the assignment of the number of electrons involved in the primary reduction process, there are significant differences between the IR spectra reported for the respective one-electron reduced product that are unlikely to be accounted for in terms of the different bridging ligands. Moreover, in terms of the short half-life of $M_{VI\text{-}A}$ (~10 s) it is surprising that the one electron reduced product of $Fe_2(\mu\text{-SEt})_2(CO)_6$ is unreactive over the timescale of preparative electrosynthesis. Further studies are needed to clarify whether the difference in the reaction products are due to subtle differences between the compounds or whether this arises from the different concentration gradients that apply in the thin-layer and bulk electrosynthetic experiments.

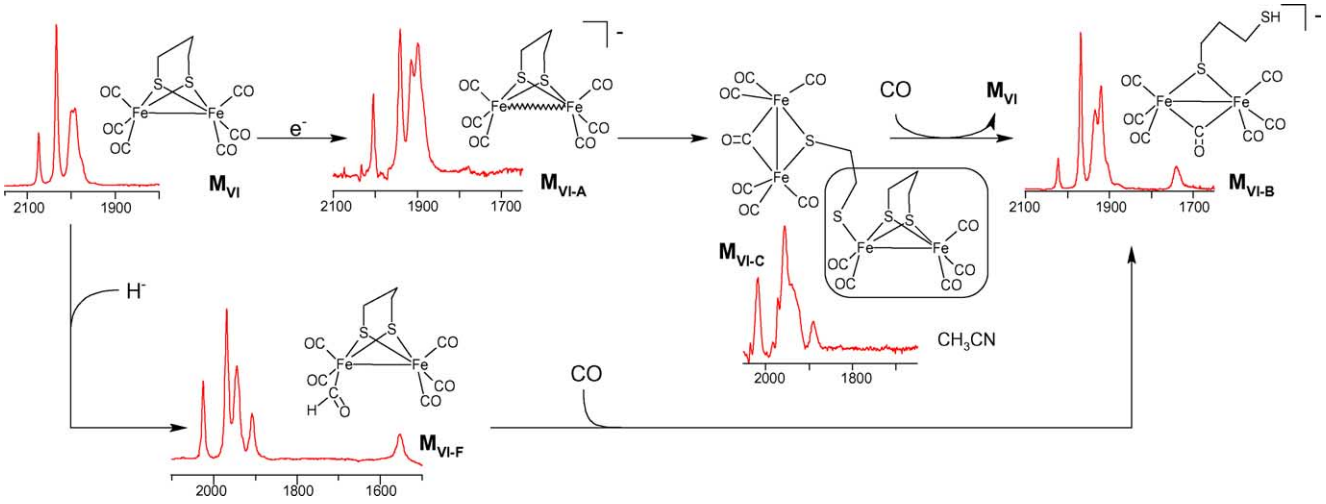

Scheme 3. Products formed following electrochemical and hydride reduction of M_{VI} [104]. IR spectra of $M_{VI\text{-}A}$, $M_{VI\text{-}B}$ and $M_{VI\text{-}C}$ were extracted from SEC experiments and the spectrum of $M_{VI\text{-}F}$ was obtained using interrupted flow techniques.

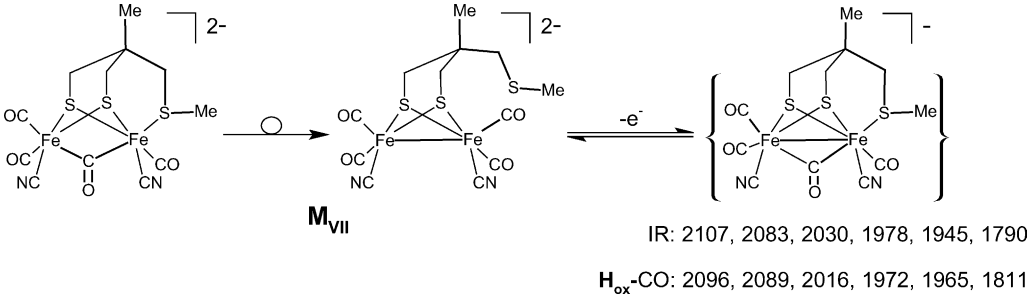

Scheme 4. Structure of M_{VII} and its proposed oxidation product. The wavenumbers of the IR bands of H_{ox}-CO were taken from [83].

Substitution of the CO ligands of M_{VI} by stronger donor ligands such as phosphine or cyanide leads to a shift of the reduction potential to more negative values and for CH_3CN the reduction wave is close to the solvent background. A good example of the changes observed in the electrochemistry is provided by the study by Darensbourg and co-workers [106] in which the phosphine is 1,3,5-triaza-7-phosphaadamantane (PTA). The mono and bis PTA substituted complexes have reduction potentials shifted more cathodic than M_{VI} by 0.2 and 0.44 V, respectively, and the reduction waves become irreversible. Protonation of the PTA ligand reduces the extent of electron donation to the diiron core and this is reflected by a shift of the reduction potentials so as to be nearly coincident with that of M_{VI}. Both for the phosphine-substituted compounds, and their protonated analogues, the reduction processes are assumed to involve one-electron steps. This assignment is based on the charge passed during bulk electrolysis [106].

Since seemingly related thiolate-bridged diiron compounds have been shown to undergo reduction by one- or two-electron processes it is important that this aspect of the electrochemistry be considered when embarking on studies of the related compounds. In terms of the available data it would appear that the identity of the bridging ligand is of more importance than substitution of the CO ligands, however at this time the experimental base is still limited.

An important characteristic of the H-cluster is the change of CO co-ordination geometry that accompanies a change of redox state. A switch between terminal and bridging CO is also implicated in CO/CN^- substitution reactions of M_{VI} [107]. The one- and two-electron reduction products of M_{VI}, $M_{VI\text{-}A}$ and $M_{VI\text{-}B}$, are of relevance since for this series of compounds related by one-electron steps only $M_{VI\text{-}B}$ includes a bridging CO group. Interest in the structure of this species is enhanced by its observed involvement in hydride transfer chemistry [104]. Whereas $M_{VI\text{-}B}$ is found to be relatively stable in the absence of dioxygen a crystalline sample suitable for crystallographic analysis was not obtained and a range of spectroscopic and chemical observations were needed to deduce the structure, this being supported by XAFS measurements. Surprisingly, two-electron reduction of M_{VI} is accompanied by the addition of CO and dissociation of one end of the pdt ligand. A summary of the chemical transformations are shown in Scheme 3, where the involvement of the dimeric species ($M_{VI\text{-}C}$) is most clearly evident in SEC experiments conducted in the absence of additional CO [104].

Recently, Rauchfuss and co-workers have reported that a family of carbonyl/isocyanide dithiolate-bridged diiron complexes undergo a terminal to bridging co-ordination change following two-electron reduction [108]. The X-ray structures of the neutral and dicationic forms, together with DFT calculations, were used to develop a description of the Fe–Fe interaction for the bridged and non-bridged forms. This paper also includes a discussion of the differences in the chemistry that result when the pdt bridge is replaced by ethane-1,2-dithiolate.

In terms of composition the compound most closely related to the H-cluster is $[Fe_2(MeSCH_2C(Me)(CH_2S)_2)(CN)_2(CO)_4]^{2-}$, M_{VII}. The monocyanide analogue has a 2Fe3S core, with the pendant thioether co-ordinated to one of the Fe atoms. Addition of a second cyanide ligand proceeds through a long-lived intermediate having a bridging CO group this rearranges by dissociation of the thioether to give a structure similar to the dicyanide derivative of M_{VI} [107]. SEC oxidation of M_{VII} at −0.25 V (versus SCE) results in the formation of a short-lived product that that can be reduced to recover the starting material. The oxidation product has an IR spectrum remarkably similar to that of H_{ox}-CO, including the presence of a bridging CO group (Scheme 4). The magnitude of the shift of the ν(CO) and ν(CN) modes is consistent with the oxidation being a one-electron process. EPR spectra obtained from ferrocenyl-oxidised samples of M_{VII} give a rhombic, $S = 1/2$, EPR spectrum [109] that is closely related to that obtained from H_{ox}-CO [110].

8. Electrocatalytic proton reduction by dithiolate-bridged diiron compounds

Biomimetic hydrogen evolution for H-cluster related compounds was first reported by Rauchfuss and co-workers [111,112]. The compounds $(CO)_2L_aFe(\mu\text{-pdt})FeL_b(CO)_2$; $L_a = L_b = PMe_3$ (M_{VIII}) and $L_a = PMe_3$, $L_b = CN^-$ (M_{IX}) are reduced at strongly cathodic potentials (∼−2 V) however protonation on the Fe–Fe bond reduces the reduction potential by ∼0.9 V. In acetonitrile M_{VIII} is protonated by *p*-toluenesulfonic acid (HOTs, pK_a 8 in CH_3CN [113]) and a weak electrocatalytic response is observed at the reduction

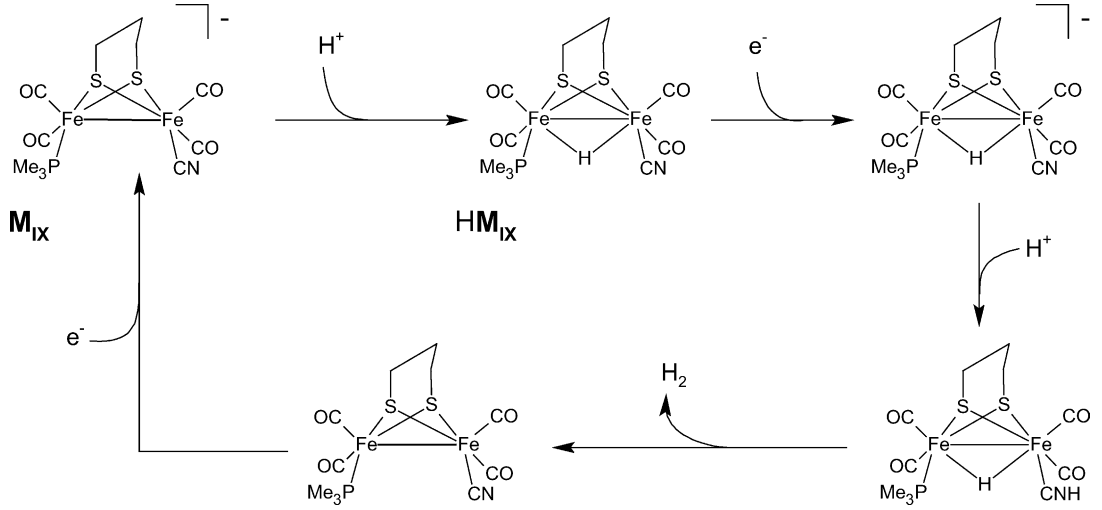

Scheme 5. Proposed mechanism for electrocatalytic proton reduction by M_{IX} (CH_3CN, HOTs) [112].

potential of the protonated form (∼−1.0 V). A second reduction wave is observed at ∼−1.35 V. A far more pronounced electrocatalytic wave is obtained for M_{IX} and this was attributed to a mechanism involving protonation of the co-ordinated cyanide. Evidence for protonation of the cyanide ligand of HM_{IX} was obtained from experiments conducted using triflic acid (pK_a 2.6 in CH_3CN [113]). Whereas HM_{IX} is not protonated by HOTs in CH_3CN reduction of the complex will increase the basicity of the co-ordinated cyanide. The reaction scheme proposed for electrocatalytic proton reduction by M_{IX} is given in Scheme 5 [112].

In their studies of electrocatalytic proton reduction Darensbourg and co-workers [43,106] have adopted a strategy that focuses on the use of the weak acid CH_3COOH (pK_a 28 in CH_3CN [113]) as the proton source. This avoids complications due to protonation of the Fe–Fe bond prior to reduction in cases where strong σ donors such as phosphines replace the CO ligands. For M_{VI} the primary reduction process at −1.34 V (versus NHE) is found not to be electrocatalytic with CH_3COOH but that there is a small increase in the cathodic current prior to the onset of a weak electrocatalytic response at −1.95 V [106]. For the phosphine-substituted compound M_{VII} reduction occurs at strongly reducing potentials (−1.85 V) but in this case the primary reduction wave is catalytic and gives a response approximately three times that of M_{VI}. It is important to note that under the same conditions HM_{VII} has a noncatalytic primary reduction but a weakly catalytic wave at −1.86 V (that is attributed to in situ formation of M_{VII}). Since HM_{VII} shows less catalytic activity in CH_3COOH than M_{VII} this suggests that protonation of the Fe–Fe bond does not lead to the formation of an active species and infers that the catalytic reaction proceeds through terminal Fe hydrides.

The more sterically demanding PTA ligands provide an insight into the subtlety of the chemistry exhibited by the system. The mono, M_X, and bis substituted, M_{XI}, PTA derivatives give irreversible one-electron reductions and two-electron oxidations that are shifted in potential by ∼−0.2 V for each PTA/CO exchange. Unlike M_{VII}, the primary reductions of both M_X and M_{XI} are electrocatalytic with CH_3COOH, albeit weakly. Protonation of the PTA ligand gives H_2M_{XI} and the reduction of this compound occurs at a more positive potential (−1.35 V). In this case the primary reduction wave is not catalytic but an electrocatalytic wave is obtained at potentials similar to those of M_{XI}. SEC monitoring of the reduction of H_2M_{XI} at mild potentials results in formation of M_{XI}. Methylation of the PTA ligand has a similar effect on the ν(CO) modes as protonation and the reduction potential of $(Me_2)M_{XI}$ (−1.46 V) is a little higher than that of H_2M_{XI}. However, the primary reduction wave of $(Me_2)M_{XI}$ is weakly electrocatalytic with CH_3COOH. There is a suggestion, based on the electrochemical response, that demethylation of the ligand occurs during the course of the reaction. It was noted that the voltammetry obtained for solutions of M_{XI} with CH_3COOH feature curve-crossing events on the anodic scan. While this type of response is most commonly associated with the formation of an active film on the surface of the electrode, transfer of the electrode from these experiments to solutions containing supporting electrolyte and acid did not give an elevated background current. This may suggest the active catalyst is formed from irreversible reactions at strongly reducing potentials, however the form of this species remains to be identified.

The mechanism for electrocatalytic proton reduction suggested by Darensbourg and co-workers for M_{VI} [106] and $Fe_2(\mu\text{-}SEt)_2(CO)_6$ [43] in the presence of CH_3COOH involves two sequential one-electron reductions (at ∼−1.34 and ∼−2 V) followed by chemical reaction (an EECC mechanism). The chemical steps involve protonation (two times) followed by elimination of dihydrogen. This interpretation would appear to be at odds with the faster timescale thin-layer SEC experiments conducted on M_{VI} where in the presence of

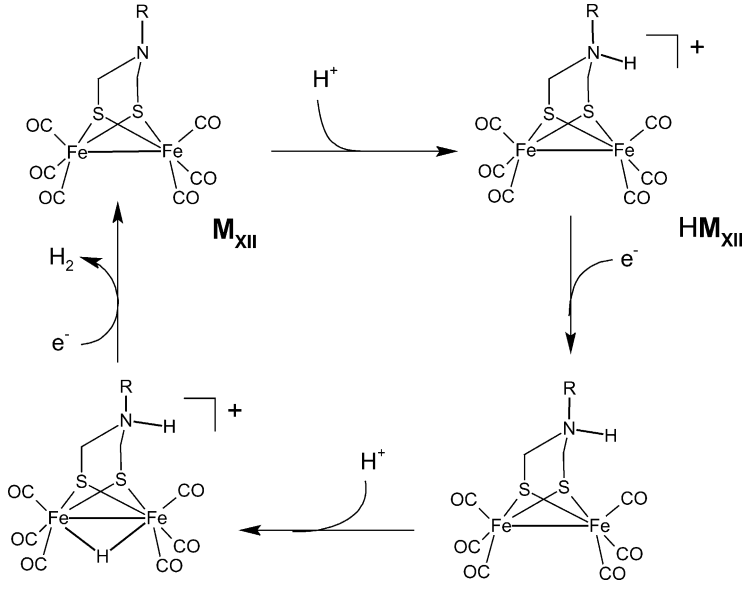

Scheme 6. Proposed scheme for electrocatalytic proton reduction by $Fe_2(\mu\text{-}(SCH_2)_2N(p\text{-}C_6H_4Br))(CO)_6$ [105].

H_2O (a weaker acid than CH_3COOH) the initial one-electron reduction process evolves into a net two-electron reaction to give $M_{VI\text{-}B}$ [104]. Similar behaviour is also observed for $Fe_2(\mu\text{-}SEt)_2(CO)_6$ [114].

For the phosphine-substituted compounds (M_{VII}–M_{XI}) electrocatalysis, where observed, is associated with the primary reduction process and in these cases an ECCE mechanism was proposed [106]. In this case one-electron reduction is followed by protonation (twice) prior to the second one-electron reduction and dihydrogen elimination.

DFT modelling of the H-cluster by Hall and co-workers led to the suggestion that the central light atom of the dithiolate bridge in the H-cluster be a N rather than the C atom as modelled in the initial structure [115,116]. This being based on a predicted lowering of the energy barrier for heterolytic cleavage and formation of dihydrogen [116]. Further analysis of the crystal structure has provided support for that proposition [8,11,82]. There is limited evidence for an increase in the rate of electrocatalytic proton reduction by model compounds that include a dta bridge compared to those incorporating a pdt group. This is provided by the substituted dta compound $Fe_2(\mu\text{-}(SCH_2)_2N(p\text{-}C_6H_4Br))(CO)_6$, M_{XII} [105]. Efficient electrocatalysis is obtained for CH_3CN solutions of M_{XII} with $HClO_4$ as the proton source. Under the conditions of the experiment the N atom of the bridge is protonated (as shown by IR, NMR and UV–vis spectroscopy) and this shifts of the reduction potential by ~0.4 V. The proposed mechanism for electrocatalysis is shown in Scheme 6. It should be noted that the basicity of the bridging N atom is not high, and the *N*-phenyl analogue of M_{XII} is not protonated by $HClO_4$ in CH_3CN.

The reaction schemes so far discussed account for particular spectroscopic or electrochemical observations, but in none of these cases has the mechanism been shown to be capable of yielding satisfactory simulations of the electrochemical response. Electrocatalytic proton reduction by M_{VI} in THF/HOTs gives a well-defined voltammetric response which features two distinct catalytic waves designated processes I and II (Fig. 9a) [104]. The shift of the primary reduction wave to more positive potentials following the addition of acid is due to protonation of the primary reduction product of M_{VI} and this is a clear indication of an EC reaction. It is clear from experiments conducted at lower acid concentrations (or slow scan speeds) that turnover of protons occurs at potentials associated with process I. Since the SEC experiments described earlier (Section 7) have shown that at mild potentials M_{VI} is reduced by two electrons to give $M_{VI\text{-}B}$, turnover is proposed to occur by an ECEC reaction. Process II becomes important at higher acid concentrations and this is clearly associated with a more highly reduced species. A reaction scheme taking into account these features is shown in Fig. 9c and a simulation of the electrochemistry based on this scheme is given in Fig. 9b. While the reaction scheme is relatively complicated, and potentially introduces a large number of variables into the simulation, the dependence of the voltammetry on the (i) scan rate, (ii) acid and (iii) metal complex concentration constitutes a complex data set that can be used to test the validity of the mechanism. An example of the insights that the SEC experiments can have to the development of the mechanism is provided by the identification of the path leading to deactivation of the catalyst. Our initial simulations were based on a reaction involving the two electron, one proton product ($1H^-$) however simulations based on that scheme gave a much poorer estimate of the relative importance of Process I and Process II. The path involving dimerisation is second order in the concentration of 1^- (=$M_{VI\text{-}A}$) and this is consistent with lifetime measurements of $M_{VI\text{-}A}$ in SEC experiments, moreover, the structure

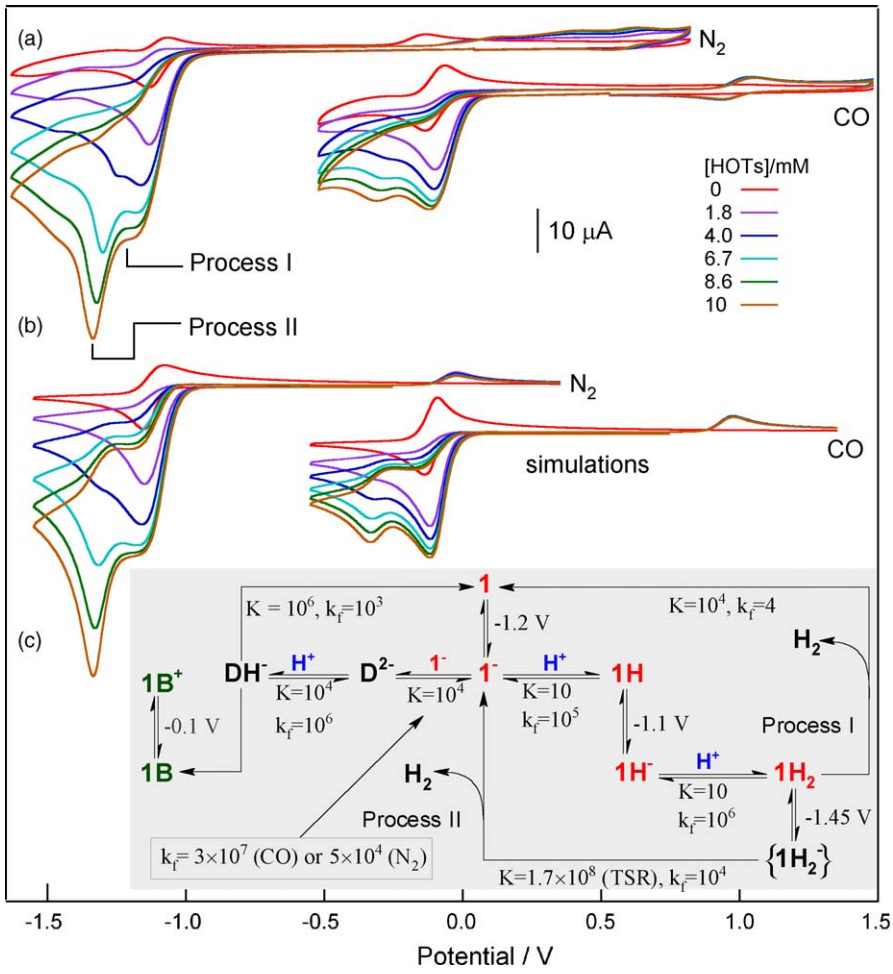

Fig. 9. Electrocatalytic proton reduction by M_{VI} in THF (a) 1 mM with 0–10 mM HOTs under an atmosphere of either N_2 or CO (an offset of 1 V has been added to the potentials of the voltammograms recorded, or simulated, under CO), (b) simulation of the voltammetry (DigiSim [117]) using the scheme given in (c). Note that the nomenclature used to describe the species differs from that used in the text; 1 corresponds to M_{VI} and D represents a dimer related to $M_{VI\text{-}C}$. A discussion of the parameters used in the simulations is given in [104]. Adapted from [104].

of $M_{VI\text{-}C}$ (Scheme 3) is readily understood if formation of the kinetic dead-end product $M_{VI\text{-}B}$ proceeds through a dimeric precursor.

In order to establish whether there is a connection between the chemistry of the H-cluster and that of the dithiolate-bridged diiron compounds during electrocatalytic proton reduction it is necessary to delineate the structures of the reactive intermediates, for the scheme shown in Fig. 9c this would correspond to 1H, $1H^-$ and $1H_2$. IR-SEC experiments conducted on a solution of M_{VI} with seven equivalents of HOTs give an apparent slow rate of reduction. Despite a high current flow, the net conversion of M_{VI} into $M_{VI\text{-}B}$ only occurs following the depletion of acid. IR spectra recorded during the reduction are dominated by M_{VI}, together with $M_{VI\text{-}B}$ and small amounts of $M_{VI\text{-}C}$ all of which are present in experiments conducted in the absence of acid. An additional product is formed in low concentration during the reduction, $M_{VI\text{-}cat}$, and this gives the spectrum shown in Fig. 10 [104]. While it is not yet confirmed that $M_{VI\text{-}cat}$ is a catalytically important species this observation

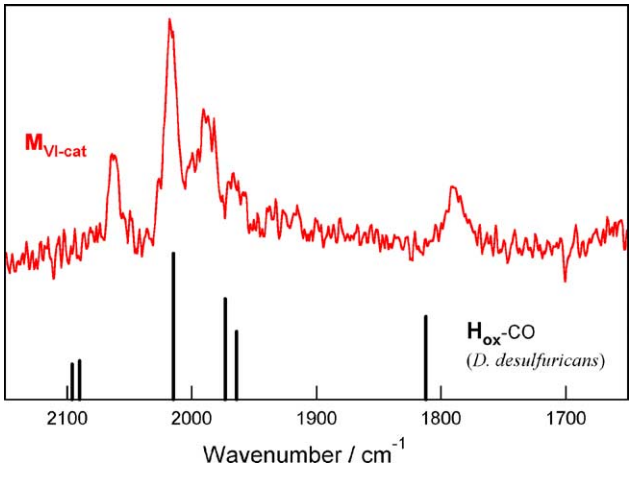

Fig. 10. IR spectra of the intermediate formed during reduction of M_{VI} in the presence of 7 equiv. of HOTs. The stick representation of the IR spectrum of H_{ox}-CO is based on the IR spectrum given in [83]. Adapted from [118].

is tantalizing because it suggests that a CO-bridged intermediate is also important during electrocatalytic proton reduction. Moreover, the electron richness of this species, as estimated by the ν(CO) bands of the terminal CO groups, is not significantly different from that of H_{ox}-CO (Fig. 10).

9. Concluding remarks

The [NiFe]-and [FeFe]-hydrogenases provide active sites that are ideally suited for study by IR-SEC techniques. The studies by de Lacey, Fernandez, Albracht and co-workers of the enzymes outlined in Sections 4 and 6 reveal detailed insights into the various levels and their associated levels of protonation, which together with the identification of the modes of CO co-ordination provide a framework for the development of a detailed molecular description of the catalytic cycle. These studies also provide a benchmark against which the so-called model systems must be judged. Whereas the SEC studies of the [NiFe]-hydrogenases have yielded richer results than the corresponding studies of the [FeFe]-hydrogenases, progress towards close synthetic models of the H-cluster has been more rapid than for the corresponding NiFe centre. It is clear from the investigations into the chemistry of M_{VI} that a complex series of reactions follow redox activation and, further, that relatively subtle changes to the basic compound can lead to substantial changes in the chemistry. This is well demonstrated by the elegant studies of Rauchfuss and Darensbourg of electrocatalytic proton reduction by substituted dithiolate-bridged diiron carbonyls, but is also evident in the dramatic changes in chemistry that accompany a change of the bridging ligand. While the delineation of this chemistry has proved to be difficult owing to the transiently stable nature of the products, the CO and cyanide groups that are central to the enzymes and models thereof bring into play a powerful range of SEC techniques. In the context of this problem IR spectroscopy holds centre stage.

Acknowledgments

SPB thanks and gratefully acknowledges the contributions of a number of postgraduate students to this research, most particularly to Kylie Vincent, Stacey Borg, Michael Cheah and Mark Bondin. Our work in this area has benefited enormously from our ongoing collaboration with Professor Chris Pickett and his research group at JIC, most notably Mathieu Razavet, Saad Ibrahim and Xiaoming Liu. The Australian Research Council is thanked both for funding this research and for providing an International Research Exchange Program grant (with CJP).

References

[1] M.W.W. Adams, Biochim. Biophys. Acta 1020 (1990) 115.
[2] M.W.W. Adams, E.I. Stiefel, Curr. Opin. Chem. Biol. 4 (2000) 214.
[3] M. Frey, Struct. Bond. 90 (1998) 98.
[4] S.P. Albracht, J. Biochim. Biophys. Acta 1188 (1994) 167.
[5] S.P.J. Albracht, Biochem. Physiol. Anaerobic Bacteria (2003) 20.
[6] P.M. Vignais, B. Billoud, J. Meyer, FEMS Microbiol. Rev. 25 (2001) 455.
[7] P.M. Vignais, A. Colbeau, Curr. Issues Mol. Biol. 6 (2004) 159.
[8] Y. Nicolet, C. Cavazza, J.C. Fontecilla-Camps, J. Inorg. Biochem. 91 (2002) 1.
[9] F.A. Armstrong, Curr. Opin. Chem. Biol. 8 (2004) 133.
[10] J.C. Fontecilla-Camps, M. Frey, E. Garcin, C. Hatchikian, Y. Montet, C. Piras, X. Vernede, A. Volbeda, Biochimie 79 (1997) 661.
[11] Y. Nicolet, B.J. Lemon, J.C. Fontecilla-Camps, J.W. Peters, Trends Biochem. Sci. 25 (2000) 138.
[12] J.-C. Fontecilla-Camps, M. Frey, E. Garcin, Y. Higuchi, Y. Montet, Y. Nicolet, A. Volbeda, in: R. Cammack, M. Frey, R.L. Robson (Eds.), Hydrogen as a Fuel, Taylor & Francis, London, 2001, pp. 93, 238.
[13] A. Volbeda, J.C. Fontecilla-Camps, J. Chem. Soc., Dalton Trans. (2003) 4030.
[14] D.J. Evans, C. Pickett, J. Chem. Soc. Rev. 32 (2003) 268.
[15] C.L. Drennan, J.W. Peters, Curr. Opin. Struct. Biol. 13 (2003) 220.
[16] A. Volbeda, E. Garcin, C. Piras, A.L. de Lacey, V.M. Fernandez, E.C. Hatchikian, M. Frey, J.C. Fontecilla-Camps, J. Am. Chem. Soc. 118 (1996) 12989.
[17] J.W. Peters, W.N. Lanzilotta, B.J. Lemon, L.C. Seefeldt, Science 282 (1998) 1853.
[18] Y. Nicolet, C. Piras, P. Legrand, C.E. Hatchikian, J.C. Fontecilla-Camps, Structure 7 (1999) 13.
[19] G. Buurman, S. Shima, R.K. Thauer, FEBS Lett. 485 (2000) 200.
[20] E.J. Lyon, S. Shima, R. Boecher, R.K. Thauer, F.-W. Grevels, E. Bill, W. Roseboom, S.P.J. Albracht, J. Am. Chem. Soc. 126 (2004) 14239.
[21] A. Volbeda, M.-H. Charon, C. Piras, E.C. Hatchikian, M. Frey, J.C. Fontecilla-Camps, Nature 373 (1995) 580.
[22] K.A. Bagley, E.C. Duin, W. Roseboom, S.P.J. Albracht, W.H. Woodruff, Biochemistry 34 (1995) 5527.
[23] K.A. Bagley, C.J. Van Garderen, M. Chen, W.H. Woodruff, E.C. Duin, S.P.J. Albracht, Biochemistry 33 (1994) 9229.
[24] R.P. Happe, W. Roseboom, A.J. Pierik, S.P. Albracht, K.A. Bagley, Nature 385 (1997) 126.
[25] K. Nakamoto, Infrared and Raman Spectra of Inorganic and Coordination Compounds, Part A: Theory and Applications in Inorganic Chemistry, 5th ed., Wiley, New York, 1997.
[26] P.S. Braterman, Metal Carbonyl Spectra, Academic Press, London, 1975.
[27] E. Münck, Phys. Methods Bioinorg. Chem. (2000) 287.
[28] H.H. Zhang, B. Hedman, K.O. Hodgson, in: E.I. Solomon, A.B.P. Lever (Eds.), Inorganic Electronic Structure and Spectroscopy, vol. 1, Wiley, New York, 1999, p. 513.
[29] J. Robinson, Specialist Periodical Report on Electrochemistry, vol. 9, Royal Society of Chemistry, London, 1984, p. 101.
[30] R.J. Gale (Ed.), Spectroelectrochemistry: Theory and Practice, Plenum Press, New York, 1988.
[31] J.A. Crayston, Compr. Coordin. Chem. II 1 (2004) 775.
[32] P.A. Christensen, A. Hamnett, Techniques and Mechanisms in Electrochemistry, Blackie Academic and Professional, London, 1994.
[33] C.H. Hamann, A. Hamnett, W. Vielstich, Electrochemistry, Wiley/VCH, Weinheim, 1998.
[34] R.W. Murray, W.R. Heineman, G.W. O'Dom, Anal. Chem. 39 (1967) 1666.
[35] M. Witek, J. Wang, J. Stotter, M. Hupert, S. Haymond, P. Sonthalia, G.M. Swain, J.K. Zak, Q. Chen, D.M. Gruen, J.E. Butler, K. Kobashi, T. Tachibana, J. Wide Bandgap Mater. 8 (2002) 171.
[36] J. Stotter, J. Zak, Z. Behler, Y. Show, G.M. Swain, Anal. Chem. 74 (2002) 5924.

[37] D. Moss, E. Nabedryk, J. Breton, W. Maentele, Eur. J. Biochem. 187 (1990) 565.
[38] A.L. de Lacey, E.C. Hatchikian, A. Volbeda, M. Frey, J.C. Fontecilla-Camps, V.M. Fernandez, J. Am. Chem. Soc. 119 (1997) 7181.
[39] W.N. Hansen, R.A. Osteryoung, T. Kuwana, J. Am. Chem. Soc. 88 (1966) 1062.
[40] S.P. Best, R.J.H. Clark, R.C.S. McQueen, R.P. Cooney, Rev. Sci. Instrum. 58 (1987) 2071.
[41] S.J. Borg, S.P. Best, J. Electroanal. Chem. 535 (2002) 57.
[42] H.B. Martin, P.W. Morrison Jr., Electrochem. Solid-State Lett. 4 (2001) E17.
[43] D. Chong, I.P. Georgakaki, R. Mejia-Rodriguez, J. Sanabria-Chinchilla, M.P. Soriaga, M.Y. Darensbourg, J. Chem. Soc., Dalton Trans. (2003) 4158.
[44] M.J. Maroney, M.A. Pressler, S.A. Mirza, J.P. Whitehead, R.J. Gurbiel, B.M. Hoffman, Adv. Chem. Ser. 246 (1995) 21.
[45] S.P.J. Albracht, P. Bertrand, B. Bleijlevens, F. Dole, B. Guigliarelli, W.R. Hagen, R.P. Happe, W. Lubitz, M.J. Maroney, C. Massanz, J.J.G. Moura, A.S. Pereira, A.J. Pierik, O. Sorgenfrei, M. Stein, P. Tavares, in: R. Cammack, M. Frey, R.L. Robson (Eds.), Hydrogen as a Fuel, Taylor & Francis, London, 2001, p. 110, 238.
[46] W. Lubitz, M. Brecht, S. Foerster, M. van Gastel, M. Stein, ACS Symp. Ser. 858 (2003) 128.
[47] S.P. Albracht, J. Biochem. Soc. Trans. 13 (1985) 582.
[48] R. Cammack, V.M. Fernandez, K. Schneider, Biochimie 68 (1986) 85.
[49] R. Cammack, M. Fernandez Victor, K. Schneider, in: J.R.J. Lancaster (Ed.), The Bioinorganic Chemistry of Nickel, VCH, New York, 1988, p. 167.
[50] J.G. Moura, M. Teixeira, I. Moura, L. Jean, in: J.R.J. Lancaster (Ed.), The Bioinorganic Chemistry of Nickel, VCH, New York, 1988, p. 191.
[51] F. Dole, A. Fournel, V. Magro, E.C. Hatchikian, P. Bertrand, B. Guigliarelli, Biochemistry 36 (1997) 7847.
[52] C. Bagyinka, J.P. Whitehead, M.J. Maroney, J. Am. Chem. Soc. 115 (1993) 3576.
[53] J.J.G. Moura, I. Moura, B.H. Huynh, H.J. Krueger, M. Teixeira, R.C. DuVarney, D.V. DerVartanian, A.V. Xavier, H.D. Peck Jr., J. LeGall, Biochem. Biophys. Res. Commun. 108 (1982) 1388.
[54] M. Teixeira, I. Moura, A.V. Xavier, H. Huynh Boi, D.V. DerVartanian, H.D. Peck Jr., J. LeGall, J.J.G. Moura, J. Biol. Chem. 260 (1985) 8942.
[55] L.M. Roberts, P.A. Lindahl, Biochemistry 33 (1994) 14339.
[56] L.M. Roberts, P.A. Lindahl, J. Am. Chem. Soc. 117 (1995) 2565.
[57] R. Cammack, D. Patil, R. Aguirre, E.C. Hatchikian, FEBS Lett. 142 (1982) 289.
[58] F.A. Cotton, G. Wilkinson, Advanced Inorganic Chemistry: A Comprehensive Text, 5th ed., Wiley/Interscience, 1988, p. 1035.
[59] J.M.C.C. Coremans, J.W. Van der Zwaan, S.P.J. Albracht, Biochim. Biophys. Acta 997 (1989) 256.
[60] A.L. de Lacey, A. Pardo, V.M. Fernandez, S. Dementin, G. Adryanczyk-Perrier, E.C. Hatchikian, M. Rousset, J. Biol. Inorg. Chem. 9 (2004) 636.
[61] A.L. de Lacey, C. Stadler, V.M. Fernandez, E.C. Hatchikian, H.-J. Fan, S. Li, M.B. Hall, J. Biol. Inorg. Chem. 7 (2002) 318.
[62] B. Bleijlevens, F.A. Broekhuizen, A.L. Lacey, W. Roseboom, V.M. Fernandez, S.P.J. Albracht, J. Biol. Inorg. Chem. 9 (2004) 743.
[63] S. Foerster, M. Stein, M. Brecht, H. Ogata, Y. Higuchi, W. Lubitz, J. Am. Chem. Soc. 125 (2003) 83.
[64] M. Carepo, D.L. Tierney, C.D. Brondino, T.C. Yang, A. Pamplona, J. Telser, I. Moura, J.J.G. Moura, B.M. Hoffman, J. Am. Chem. Soc. 124 (2002) 281.
[65] Y. Higuchi, H. Ogata, K. Miki, N. Yasuoka, T. Yagi, Structure 7 (1999) 549.
[66] A.K. Jones, S.E. Lamle, H.R. Pershad, K.A. Vincent, S.P.J. Albracht, F.A. Armstrong, J. Am. Chem. Soc. 125 (2003) 8505.
[67] C. Stadler, A.L. de Lacey, Y. Montet, A. Volbeda, J.C. Fontecilla-Camps, J.C. Conesa, V.M. Fernandez, Inorg. Chem. 41 (2002) 4424.
[68] S.E. Lamle, S.P.J. Albracht, F.A. Armstrong, J. Am. Chem. Soc. 126 (2004) 14899.
[69] S. Kurkin, S.J. George, R.N.F. Thorneley, S.P.J. Albracht, Biochemistry 43 (2004) 6820.
[70] S.J. George, S. Kurkin, R.N.F. Thorneley, S.P.J. Albracht, Biochemistry 43 (2004) 6808.
[71] B. Guigliarelli, C. More, A. Fournel, M. Asso, E.C. Hatchikian, R. Williams, R. Cammack, P. Bertrand, Biochemistry 34 (1995) 4781.
[72] H. Ogata, Y. Mizoguchi, N. Mizuno, K. Miki, S.-i. Adachi, N. Yasuoka, T. Yagi, O. Yamauchi, S. Hirota, Y. Higuchi, J. Am. Chem. Soc. 124 (2002) 11628.
[73] G. Davidson, S.B. Choudhury, Z. Gu, K. Bose, W. Roseboom, S.P.J. Albracht, M.J. Maroney, Biochemistry 39 (2000) 7468.
[74] A.C. Marr, D.J.E. Spencer, M. Schroder, Coordin. Chem. Rev. 219–221 (2001) 1055.
[75] P. Christopher, J. Coordin. Chem. Rev., in this issue.
[76] L.L. Efros, H.H. Thorp, G.W. Brudvig, R.H. Crabtree, Inorg. Chem. 31 (1992) 1722.
[77] C.J. Curtis, A. Miedaner, R. Ciancanelli, W.W. Ellis, B.C. Noll, M.R. DuBois, D.L. DuBois, Inorg. Chem. 42 (2003) 216.
[78] D. Sellmann, R. Prakash, F.W. Heinemann, Eur. J. Inorg. Chem. (2004) 1847.
[79] Q. Wang, J.E. Barclay, A.J. Blake, E.S. Davies, D.J. Evans, A.C. Marr, E.J.L. McInnes, J. McMaster, C. Wilson, M. Schröder, Chem. Eur. J. 10 (2004) 3384.
[80] D. Sellmann, F. Lauderbach, F. Geipel, F.W. Heinemann, M. Moll, Angew. Chem., Int. Ed. 43 (2004) 3141.
[81] A.J. Pierik, M. Hulstein, W.R. Hagen, S.P.J. Albracht, Eur. J. Biochem. 258 (1998) 572.
[82] Y. Nicolet, A.L. de Lacey, X. Vernede, V.M. Fernandez, E.C. Hatchikian, J.C. Fontecilla-Camps, J. Am. Chem. Soc. 123 (2001) 1596.
[83] A.L. de Lacey, C. Stadler, C. Cavazza, E.C. Hatchikian, V.M. Fernandez, J. Am. Chem. Soc. 122 (2000) 11232.
[84] B.J. Lemon, J.W. Peters, Biochemistry 38 (1999) 12969.
[85] Z. Chen, B.J. Lemon, S. Huang, D.J. Swartz, J.W. Peters, K.A. Bagley, Biochemistry 41 (2002) 2036.
[86] B.J. Lemon, J.W. Peters, J. Am. Chem. Soc. 122 (2000) 3793.
[87] T.B. Rauchfuss, Inorg. Chem. 43 (2004) 14.
[88] M.Y. Darensbourg, E.J. Lyon, J.J. Smee, Coord. Chem. Rev. 206–207 (2000) 533.
[89] H. Reihlen, A. van Friedolsheim, W. Oswald, Annal 465 (1928) 72.
[90] E.J. Lyon, I.P. Georgakaki, J.H. Reibenspies, M.Y. Darensbourg, Angew. Chem., Int. Ed. 38 (1999) 3178.
[91] M. Schmidt, S.M. Contakes, T.B. Rauchfuss, J. Am. Chem. Soc. 121 (1999) 9736.
[92] F. Gloaguen, J.D. Lawrence, M. Schmidt, S.R. Wilson, T.B. Rauchfuss, J. Am. Chem. Soc. 123 (2001) 12518.
[93] H. Li, T.B. Rauchfuss, J. Am. Chem. Soc. 124 (2002) 726.
[94] A.L. Cloirec, S.C. Davies, D.J. Evans, D.L. Hughes, C.J. Pickett, S.P. Best, S. Borg, Chem. Commun. (1999) 2285.
[95] M. Razavet, S.C. Davies, D.L. Hughes, C.J. Pickett, Chem. Commun. (2001) 847.
[96] W.-F. Liaw, N.-H. Lee, C.-H. Chen, C.-M. Lee, G.-H. Lee, S.-M. Peng, J. Am. Chem. Soc. 122 (2000) 488.
[97] W.-F. Liaw, W.-T. Tsai, H.-B. Gau, C.-M. Lee, S.-Y. Chou, W.-Y. Chen, G.-H. Lee, Inorg. Chem. 42 (2003) 2783.
[98] J.D. Lawrence, H. Li, T.B. Rauchfuss, M. Benard, M.-M. Rohmer, Angew. Chem., Int. Ed. 40 (2001) 1768.
[99] J.D. Lawrence, H. Li, T.B. Rauchfuss, Chem. Commun. (2001) 1482.
[100] A. Darchen, H. Mousser, H. Patin, Chem. Commun. (1988) 968.

[101] J.P. Collman, R.K. Rothrock, R.G. Finke, E.J. Moore, F. Rose-Munch, Inorg. Chem. 21 (1982) 146.
[102] R.E. Dessy, R.L. Kornmann, C. Smith, R. Haytor, J. Am. Chem. Soc. 90 (1968) 2001.
[103] J.-F. Capon, F. Gloaguen, P. Schollhammer, J. Talarmin, J. Electroanal. Chem. 566 (2004) 241.
[104] S.J. Borg, T. Behrsing, S.P. Best, M. Razavet, X. Liu, C.J. Pickett, J. Am. Chem. Soc. 126 (2004) 16988.
[105] S. Ott, M. Kritikos, B. Åkermark, L. Sun, R. Lomoth, Angew. Chem., Int. Ed. 43 (2004) 1006.
[106] R. Mejia-Rodriguez, D. Chong, J.H. Reibenspies, M.P. Soriaga, M.Y. Darensbourg, J. Am. Chem. Soc. 126 (2004) 12004.
[107] S.J. George, Z. Cui, M. Razavet, C.J. Pickett, Chem. Eur. J. 8 (2002) 4037.
[108] C.A. Boyke, T.B. Rauchfuss, S.R. Wilson, M.-M. Rohmer, M. Benard, J. Am. Chem. Soc. 126 (2004) 15151.
[109] M. Razavet, S.J. Borg, S.J. George, S.P. Best, S.A. Fairhurst, C.J. Pickett, Chem. Commun. (2002) 700.
[110] M.W.W. Adams, J. Biol. Chem. 262 (1987) 15054.
[111] F. Gloaguen, J.D. Lawrence, T.B. Rauchfuss, J. Am. Chem. Soc. 123 (2001) 9476.
[112] F. Gloaguen, J.D. Lawrence, T.B. Rauchfuss, M. Bénard, M.-M. Rohmer, Inorg. Chem. 41 (2002) 6573.
[113] K. Izutsu, Acid-Base Dissociation Constants in Dipolar Aprotic Solvents, Blackwell Scientific Publications, Oxford, 1990.
[114] S.J. Borg, S.P. Best, Unpublished results.
[115] Z. Cao, M.B. Hall, J. Am. Chem. Soc. 123 (2001) 3734.
[116] H.-J. Fan, M.B. Hall, J. Am. Chem. Soc. 123 (2001) 3828.
[117] M. Rudolph, D.P. Reddy, S.W. Feldberg, Anal. Chem. 66 (1994) 589A.
[118] S.J. Borg, M.I. Bondin, S.P. Best, M. Razavet, X. Liu, C.J. Pickett, Biochem. Soc. Trans. 33 (2005) 3–6.